Diagnostics for characterisation of plasma actuators

Topical Review

Diagnostics for characterisation of plasma actuators

Marios Kotsonis

Delft University of technology, Kluyverweg 2, Delft 2629HS, The Netherlands

E-mail: m.kotsonis@tudelft.nl

CrossMark

Abstract

The popularity of plasma actuators as flow control devices has sparked a flurry of diagnostic efforts towards their characterisation. This review article presents an overview of experimental investigations employing diagnostic techniques specifically aimed at AC dielectric barrier discharge, DC corona and nanosecond pulse plasma actuators. Mechanical, thermal and electrical characterisation techniques are treated. Various techniques for the measurement of induced velocity, body force, heating effects, voltage, current, power and discharge morphology are presented and common issues and challenges are described. The final part of this report addresses the effect of ambient conditions on the performance of plasma actuators.

Keywords: plasma actuator, diagnostics, measurement, velocity, force, power

(Some figures may appear in colour only in the online journal)

1. Introduction

Aristotle introduces the concept of ὃ οὐ κινούμενον κινεῖ (*the unmoved mover*) in his Metaphysics treatise [1]. As implied by the name, the unmoved mover is the one that can move others while it itself stays still. A modern equivalent is the technology of plasma actuators [2, 3]. They have received overwhelming attention from the flow control community during the past 15 years. This is mainly attributed to their inherent features, which render them ideal for active flow control. They are relatively easy to manufacture, operate with low power consumption, exhibit high frequency response and, as modern *unmoved movers*, have no moving parts. On the other hand their flow control authority is still limited and efficient scaling to operation at high Reynolds numbers is challenging. The improvement of plasma actuator performance has been one of the major driving factors behind the vast number of characterisation studies published.

Several variations of plasma actuators exist such as non-thermal alternating current dielectric barrier discharge (AC-DBD) [4], direct current corona (DC-corona) [5], nanosecond pulsed dielectric barrier discharge (ns-DBD) [6], and arc filament actuators [7]. This review is focused on experimental diagnostics for characterisation of AC-DBD, DC-corona and ns-DBD actuators.

1.1. Corona discharge

DC-corona discharge occurs under sufficiently large electric fields near sharp metallic points. It forms part of the more general Townsend discharge and can be perceived as a weakly luminous glow, localised near the high voltage tip [8, 9]. This discharge can be ignited with a relatively high voltage near one of the electrodes. While still in glow mode the plasma temperature is low, almost in thermal equilibrium to the surrounding gas. If the voltage is further increased, the discharge transitions to a spark or arc with a corresponding increase of temperature. Corona discharges have found many industrial applications such as material processing and air pollution control due to their ability to generate a high concentration of radicals at atmospheric pressures without heating up the surrounding gas [9].

A typical geometric arrangement of the electrodes for DC-corona discharges is the point-to-plane volume configuration, where a metallic high voltage (HV) needle is suspended above a metallic plate acting as the ground plane. The corona is defined as negative or positive respective to the polarity of the needle electrode. The mechanism of breakdown and sustained gas ionisation depends on the type of corona. In the case of positive corona, electrons are produced by photoionisation in the air gap and drift towards the positive electrode causing an avalanche. The ions are repelled towards the grounded electrode via Coulomb forces. In contrast, the case of negative corona is more similar to the typical Townsend breakdown mechanism where electrons are created and emitted by the HV electrode and drift towards the ground. Comprehensive monographs on the subject can be found in Loeb [10] and Goldman and Goldman [11].

One of the most interesting phenomena related to corona discharges is the so-called *electric wind*, *ionic wind* or *electric aura*. The seminal work of Robinson [12, 13] refers to electric wind as 'the movement of gas induced by the repulsion of ions from the neighbourhood of a high voltage discharge electrode'. The effect is one of the earliest observed manifestations of discharges in gases. While the earliest recorded observation of the corona discharge is attributed to Otto von Guericke [14] and his frictional machine in 1672 (figure 1), it was not until 1709 that the curator of instruments for the Royal Society of London, Francis Hauksbee [15] first observed the electric wind. Following the discovery, the phenomenon has been widely studied in the eighteenth and nineteenth century. After an intermediate period of neglect, renewed interest appeared in the second half of the twentieth century due to possible applications to micropumps, high-voltage generators, electronics etc.

The electric wind was first explained by Faraday in 1838 [16]. It is simply the movement of air induced by momentum transfer due to collisions of moving ions and neutrals in the discharge volume. A variation of the point-to-plane electrode arrangement capable of directing the electric wind parallel to a wall is the wire-to-wire configuration where thin parallel wires are placed flush with or above a solid surface. In fact such configuration has been already used in 1968 by Velkof *et al* [17] in a laminar boundary layer control study. Few other studies were published in the following decades by Velkov *et al* [18], Malik *et al* [19] on turbulent drag reduction and Noger *et al* [20] on flow around a cylinder. The majority of studies on DC-corona actuators have since been published mainly by the group of University of Poitiers, France and the group of University of Buenos Aires, Argentina [5, 21].

1.2. Dielectric barrier discharge

The most popular type of plasma actuators has been the dielectric barrier discharge (DBD) actuator. Barrier discharges differ from corona discharge in the fact that one or both electrodes is encapsulated in a dielectric, insulating material. Air DBDs have a parallel history to the corona discharge. First introduced by Siemens [22] for ozone generation, their main advantage over corona discharge is their robustness towards transition
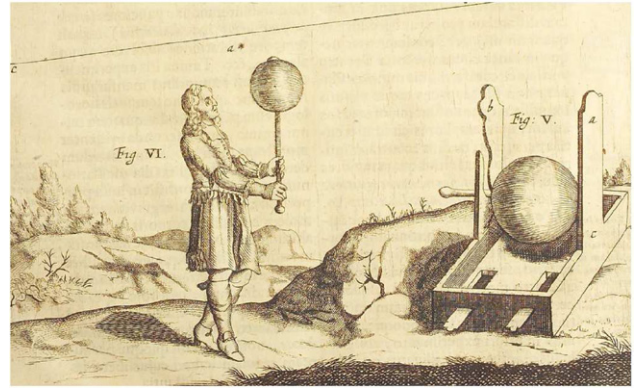

Figure 1. Otto von Guericke and his frictional electrostatic generator [14].

from glow to arc. The presence of the dielectric is the deciding factor as charge accumulates on the surface reducing the local electric field and thus quenching the discharge. This self-limiting nature of DBD is a main feature of these configurations and necessitates the use of alternating current voltage in order to sustain the plasma. The term 'plasma' was introduced by Langmuir [23] in 1928 to describe a region of gas discharge in charge equilibrium. Over the years the definition has been broadened to that of a system of particles characterised by long-range Coulomb interactions [9, 24]. An important milestone to the development of DBD has been the study of Buss [25] in which he used photographic techniques to observe the existence of microdischarges in the gap between planar electrodes for the first time. This was verified and further explained by Klemenc *et al* [26] in 1937. A further development was the operation of DBDs in atmospheric pressure air first reported by Kanazawa *et al* [27, 28], Yokohama *et al* [29] and Okazaki *et al* [30].

In general DBDs are based on the formation of microdischarges which are randomly occurring in space and time [9, 31, 32]. Their duration is in the order of few nanoseconds while the charge density and the temperature are comparable to the corona discharge. As mentioned earlier, an important feature of DBDs is the use of AC voltage. This is necessary since the dielectric does not permit DC current but only a time dependent displacement current to pass. As such, the developed streamers define conducting channels which deposit electrons onto the dielectric layer. This charge accumulation is responsible for a build-up of an opposite electric field which prevents further avalanches until the voltage is further increased or reversed [9].

Similar to the corona discharge, the DBD can have several geometric arrangements. The typical configuration using opposing symmetrical electrodes is industrially used as *volume DBD* in processes such as ozone generation, CO_2 lasers, UV excimer lamps, surface treatment and pollution control [31, 32]. An alternative configuration is the so-called *surface DBD* (SDBD) in which both electrodes are positioned on a surface and separated by the dielectric. Furthermore, if the electrodes are positioned asymmetrically the DBD is capable of inducing a net air movement similar to the corona electric wind, thus manifesting into the familiar AC-DBD plasma

actuator. The pioneering work of Roth [4, 33] was the first to observe this and simultaneously show the potential for flow control (figure 2), although mistakenly referred to the effect as glow discharge and attributed the control authority to paraelectric and peristaltic effects.

While several types of DBD actuators have branched out from the conventional AC-driven variety, a kind that has gathered considerable interest is the nanosecond-pulsed DBD actuator. Short HV pulses have been known to improve the power and stability of the corona discharge [9]. Additionally, short pulse discharges have been investigated due to the potential for enhancing combustion [34–38]. In 2008 the group of Starikovskii and co-workers [6, 39, 40] published the first studies on using a ns-DBD actuator for flow control.

1.3. Diagnostics, modelling and application of plasma actuators

The research approach towards plasma actuators has been threefold as is evident by the vast collection of related literature. Firstly, plasma actuators are investigated experimentally or numerically in various applications and flow control scenarios. These studies concentrate primarily on the control authority of the actuators and generally are concerned with the response of external flows to this kind of actuation. Their utilisation has been proposed, among others, for airfoil separation control [41–45], turbine blade separation control [46], laminar-turbulent transition delay [47], lift enhancement [48, 49], bluff body flow control [50, 51], shock wave control [52] and combustion augmentation [38]. While the most typical approach involves open-loop actuation, some closed-loop control has been demonstrated using integrated systems of sensors, actuators and controllers [53].

A second major focus point is the modelling of plasma actuators. Due to the complexity of the underlying phenomena governing the formation of the discharge, dynamics of plasma and interaction with the flow, it quickly became evident that robust and accurate representational models of the plasma actuator behaviour are of great importance. Several studies have focused on numerical models of the plasma actuator featuring varying levels of fidelity from simple phenomenological representations [54], lumped element circuit modelling [55] to complex multi-species electro-hydrodynamic simulations [56–58].

Last, but not least, an ever-increasing amount of research is steered towards the measurement and characterisation of plasma actuators. These studies aim at the qualification and quantification of the salient mechanical, thermal and electrical behaviour of these devises. They are typically conducted under quiescent flow conditions, fully decoupling the actuator performance from the external flow field. Additionally, a small number of characterisation studies under external flow conditions are concerned with the interaction of the actuator with the flow.

The complexity of the underlying physical phenomena governing the formation of the plasma discharge and its interaction with the surrounding fluid pose additional challenges to the measurement of plasma actuators. A study of the existing literature reveals a variety of diagnostic techniques, which are
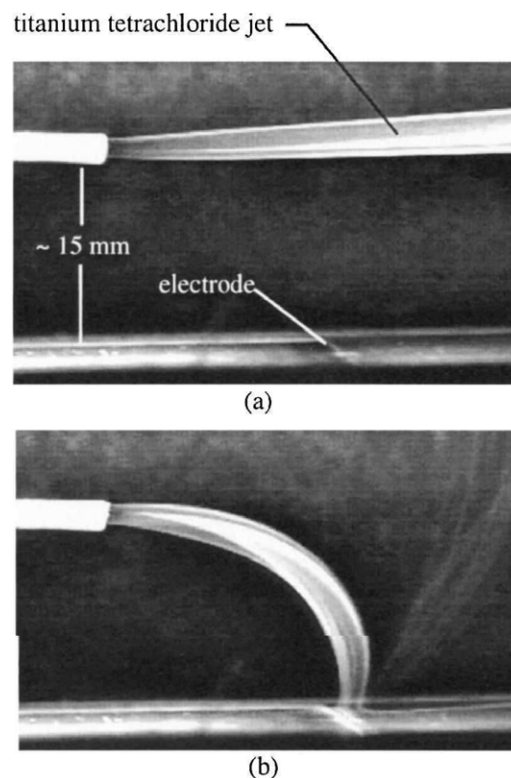

Figure 2. Flow visualisation of the one atmosphere uniform glow discharge plasma (OAUGDP), the first demonstration of flow control potential of AC-DBD plasma actuators. From [33]; reprinted by permission of the American Institute of Aeronautics and Astronautics, Inc.

chosen based on the characterisation of the desired performance aspect. Excellent reviews have holistically treated DBD plasma actuators recently [2, 3, 59–62] and the interested reader is referenced to these works for a detailed description of the plasma actuators working principles. Yet, little effort has been given to a dedicated compilation of the multitude of experimental measurement techniques employed for the characterisation of plasma actuators. This paper attempts to present these measurement techniques in a common scope. Additionally, the techniques are presented based on the measurement objective in order to provide a useful guide for experimentalists wishing to venture into plasma actuator characterisation[1]. The author would like to apologise for any studies that have accidentally been left out of this review. The vastness of existing literature on plasma actuators is indeed overwhelming.

The paper is structured as follows. The mechanical, thermal and electrical characterisation studies of the actuators are described in the three respective sections. An additional section is provided, treating the effect of ambient conditions on the performance of plasma actuators and the implications these have on the interpretation of characterisation works. The final section involves some comments on open issues and future directions in this fast growing and dynamic research field.

---

[1] The types of plasma actuators covered in this review produce and sustain weakly ionised gas. The term 'plasma' refers to this regime in the entirety of this paper.

2. Mechanical characterisation

The main attribute of plasma actuators is their ability to manipulate the flow in which they are immersed. As such, their primary function is the mechanical forcing of flows, which is characterised by measuring the response of a given flow to actuation. Although no moving parts are involved, the term *mechanical* is used here in the context of aerodynamic performance characterisation. Typically, this is done in quiescent conditions in order to clearly separate the effect of the actuator from other hydrodynamic or pressure related effects. This approach is invaluable towards better understanding the underlying physics governing the actuation. Additionally, quiescent testing can provide the ideal platform for parametric studies and optimisation of the actuator's performance.

The main features of plasma actuation in quiescent conditions depend on the type of actuator. For AC-DBD and DC-corona actuation a wall-jet structure is developed. The induced velocity (also referred to as *ionic wind* in some cases) is the product of a distributed volume body force the actuator exerts on the flow. Both velocity and body force can be measured using a variety of techniques.

For ns-DBD, the main effect of actuation is thermal. Additionally the time scales of actuation are in the order of nano- and microseconds resulting in highly dynamic effects such as the formation of weak compression waves. Techniques relying on the measurement of thermal or compressibility effects are best suited to this type of actuator. These will be treated in a subsequent section.

2.1. Induced velocity

One of the most prominent effects of plasma actuation is the development of an induced velocity jet in the vicinity of the plasma region. The jet, sometimes called *ionic wind* was first observed in 1709 [15]. Yet, it was not until the late 90s that the pioneering work of the University of Tennessee [4, 33] showed the potential for flow control. A large body of early experimental characterisation work emerged soon after the work of Roth *et al* mainly focusing on the measurement of the induced velocity. Several techniques have been applied towards accurate measurements of the developed flow. An overview of the induced velocity measurements works is presented in table 1[2].

The most straightforward and, to date, most popular technique for measuring plasma actuator-induced flows has been the use of pressure or Pitot tubes. Pressure tube measurements are a staple among experimental techniques in fluid dynamics [65]. The velocity of a given flow can be found by measuring the stagnation pressure at the open tip of the Pitot tube (figure 3). In order to minimise interference to the flow, usually thin capillary tubes are used with the open end facing the flow. The stagnation or total pressure cannot directly give the velocity. In addition, measurement of the static pressure (p_s)

is necessary. The velocity magnitude at the point of measurement (tip of Pitot tube) is then given by Bernoulli's equation:

$$p_t = p_s + \frac{1}{2}\rho V^2 \qquad (1)$$

where p_t is the total pressure measured by the Pitot tube, ρ is the density of the fluid and V is the velocity magnitude. It should be noted that simple Pitot tubes cannot provide directional information. As such, they need to be aligned to the general direction of the flow. The static pressure (p_s) is either measured by a second orifice located on the pressure tube, tangentially to the flow (Pitot-static tube) or by a static pressure probe located near the measurement area. Due to the small values of velocities involved, care should be taken regarding the location of the static pressure port and its influence on the measurement. In practice it is common to measure directly the differential between total and static pressure using analog or digital manometers.

The induced velocity achieved by AC-DBD and DC-corona actuators typically reaches maximum values of less than 10 m s^{-1} in quiescent conditions [33, 64, 66, 67]. This corresponds to differential pressure of approximately 60 Pa in sea level conditions. Considering a required accuracy of less than 0.1% (60 mPa), the need for accurate micro-manometers for this type of measurement is evident. Indeed, the vast majority of workers have been using manometers such as the Furness FC0012 [5], FC0014 [64, 68], GE Druck LPM 9481 [63], Baratron 223BD [69] or Validyne DP103-12 [67] for characterisation of both DC-corona and AC-DBD actuators.

An additional consideration is the small spatial scale of the developed wall jet due to plasma actuation. Typical wall normal distance at which the jet reaches maximum velocity (jet half-width) is in the order of a few millimetres as shown by particle image velocimetry (PIV) studies [67, 70, 71], while the streamwise extent of observable velocity is in the order of few cm (figure 4). The need for sufficient resolution of the wall jet, especially in the wall normal direction, requires the use of accurate traversing systems with a stepping resolution of tens of micrometers [33, 72, 73]. In relation to this, the inner diameter of the Pitot tube is also of importance. A Pitot tube diameter below 1 mm has been typically used in order to minimise the spatial interval in which the measurement is averaged across the velocity profile.

An important note regarding this type of measurement is the need for using non-conductive materials for the Pitot tube. This is necessary to prevent electrical arcing from the plasma region to the tip of the tube. A straightforward option is to use thin bent glass or plastic capillary tubes [74]. Even in this case static charges can be accumulated by the probe, thus affecting the electric filed. Depending on the values of applied voltage, a minimum distances of a few millimetres is advised between the tip of the tube and the plasma region.

As already mentioned, Pitot tube measurements are a simple, fast and accurate technique of establishing measurements of plasma induced velocities. The setup is relatively easy to construct and requires equipment usually found already in most laboratories, making this an ideal technique (in conjunction with electrical and thermal characterisation) for extensive parametric studies. On the other hand, the relatively low

---

[2] For all the studies presented in this paper voltage is given in peak-to-peak (p–p) values for AC-DBD actuators, amplitude values for DC-corona and pulse amplitude for ns-DBD actuators.

Table 1. Overview of induced velocity measurement works.

Steady measurements				
Reference	Technique	Voltage (p–p) [kV]	Frequency [kHz]	Notes
Roth et al (1998–2000) [4, 33]	Pitot tube	4.2–7	3	first AC-DBD study
Leger et al (2001) [5]	Pitot tube	30	DC	DC-corona
Post (2004) [90]	PIV	2–16	2–10	parametric study
Forte et al (2005) [80]	LDV	32–36	0.7	DC-corona and AC-DBD
Jacob et al (2005) [70]	PIV	10	4.5	annular actuators
Pons et al (2005) [68]	Pitot tube	20–60	0.3–1	glass dielectric
Jukes et al (2006) [76]	HWA	8	50–60	
Moreau et al (2006) [72]	Pitot tube	20–30	DC	DC-corona
Forte et al (2007) [64]	Pitot tube, LDV	16–60	0.1–2	parametric study
Kim et al (2007) [92]	PIV	11	2.6	role of oxygen
Magnier et al (2007) [74]	Pitot tube	27–44	DC	DC-corona
Santhanakrishnan and Jacob (2007) [91]	PIV	12	2.8	annular plasma synthetic jets
Moreau et al (2008) [66, 112]	Pitot tube	40	1	sliding discharge
Dong et al (2008) [63]	Pitot tube	10–20	1	array of plasma actuators
Jukes et al (2008) [79]	HWA	7.4	25	
Balcon et al (2009) [93]	PIV	40	1	
Porter et al (2009) [69]	PIV	19	5–10	non-linear actuators
Thomas et al (2009) [67]	Pitot tube, PIV	5–75	1–8	thick dielectrics
Santhanakrishnan et al (2009) [96]	PIV	12	2.8	linear plasma synthetic jets
Sosa et al (2009) [114]	Schlieren velocimetry	25	9.5	sliding discharge
Kotsonis and Veldhuis (2010) [77]	HWA	10	2	pulse operation
Kriegseis et al (2010) [94]	PIV	14–20	6.5–9.5	POD study
Durscher et al (2012) [117]	PIV	20–46	2–7	effect of dielectric temperature
Kotsonis and Ghaemi (2012) [71]	PIV	8–16	1–4	validation of force model
Dedrick et al (2013) [95]	PIV	7	5	13.5 MHz pulses
Joussot et al (2013) [82]	LDV	20	1	serrated electrodes
Unsteady measurements				
Reference	Technique	Voltage (p–p)	Frequency	Notes
Forte et al (2005) [80]	LDV	32–36	0.7	DC-corona and AC-DBD
Forte et al (2007) [64]	LDV	16–60	0.1–2	parametric study
Benard and Moreau (2010) [85]	LDV	36	0.15–1.5	multi-frequency excitations
Leonov et al (2010) [75]	Pitot tube	24	0.02–2	in air and nitrogen
Kotsonis and Ghaemi (2011) [100]	PIV	10	0.625	effect of waveform
Benard and Moreau (2012) [86]	LDV	40	1	effect of waveform
Kotsonis and Ghaemi (2012) [101]	PIV	20–40	0.6–1	asymmetric waveforms
Murphy et al [106]	PIV	7–13	2–4	
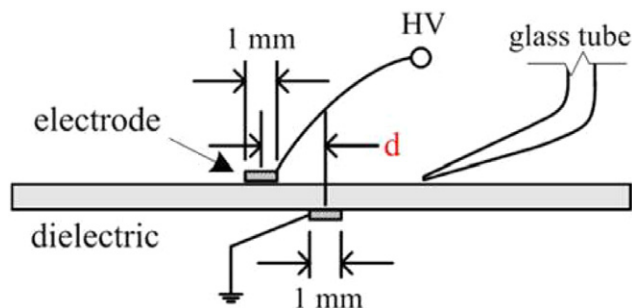
Figure 3. Pitot tube measurement setup used by Dong et al [63]. Reproduced with permission.

bandwidth of digital manometers and the phase lagging and dampening effects associated with dynamic line pressure measurements prohibit time resolved observations of the inherently fluctuating velocity field observed via other techniques such as laser doppler velocimetry (LDV) or PIV in the plasma region. An exception was demonstrated by Leonov et al [75] where a time resolved Pitot tube measurement was performed demonstrating the highly dynamic nature of the plasma induced flow. Unfortunately no specific information regarding the experimental setup was given.

A technique which has been extremely popular in classical fluid mechanics is hot wire anemometry (HWA) [78]. This method relies on thin heated sensor wires suspended in the flow. As the stream of fluid cools down the sensor, an electronic bridge circuit, increases the voltage that powers the wire in order to keep its temperature constant. By relating the bridge voltage with the velocity via pre-defined calibration
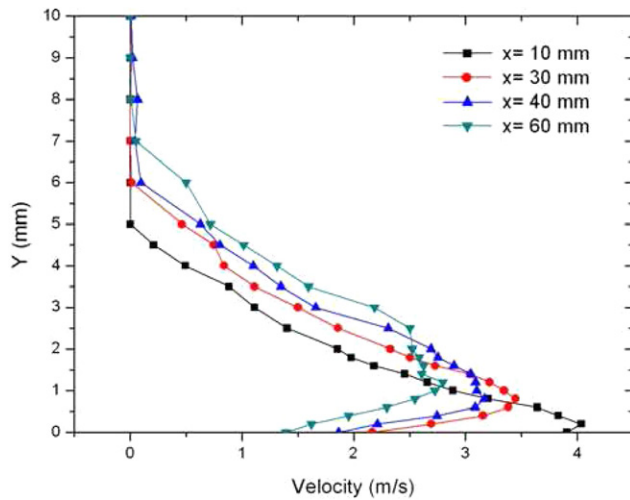
Figure 4. Velocity profiles of AC-DBD actuator measured using a Pitot tube. Reproduced from [64] with kind permission from Springer Science and Business Media.

HWA measurements of Jukes et al. [76]

HWA measurements of Kotsonis & Veldhuis [77].

Figure 5. Hot wire anemometry (HWA) measurements of AC-DBD actuators in pulse operation. (a) From [76]; reprinted by permission of the American Institute of Aeronautics and Astronautics, Inc.; (b) reproduced with permission from [77]. Copyright 2010, AIP Publishing LLC.

curves, measurements of velocity with good spatial resolution and excellent temporal response (up to 100 kHz) can be achieved. In theory this would be an ideal alternative to Pitot tube measurements for plasma actuators. In reality several issues prohibit its efficient use.

HWA has been selected for characterising DBD plasma actuators more seldom than Pitot tubes due to several inherent issues regarding hot wires and strong electric fields [46, 76, 77, 79]. An important problem is the possibility and danger of electrical arcing between the exposed electrode and the metallic hot wire probe which would destroy the latter. An additional issue is the contamination of the hot wire signal from strong electromagnetic interference (EMI) caused by the fluctuating electromagnetic field in the vicinity of the actuator. Nevertheless, both these issues can be circumvented by the use of sufficient clearance between the hot wire and the electrodes and low pass filtering, respectively. Unfortunately, the main frequency component of the EMI spectrum corresponds to the carrier frequency of actuation [77]. This also corresponds to the main frequency of velocity [80] and force [81] fluctuations in the vicinity of the actuator. Consequently, the necessary filtering diminishes the temporal resolution advantages of the hot wire technique in measuring the dynamic behaviour of the actuator (figure 5).

HWA measurements are sensitive to temperature gradients and need to be corrected for this effect. Especially for measurements near solid walls the increased heat transfer between the hot wire and the wall needs to be accounted for. In the case of plasma actuators an additional effect is a slight heating of the flow and surface due to the plasma activity [76].Careful identification of these effects and calibration of the HWA are necessary to accurately separate velocity and temperature effects.

Laser Doppler velocimetry (LDV) is a non-intrusive optical diagnostic technique enabling point velocity measurements with high spatial and temporal resolution [83, 84]. It relies on the Doppler effect whereupon two monochromatic, coherent laser beams intersect in the measurement volume. At the intersection, a series of light fringes develops at a precise wavelength. The flow is then seeded and the light scattering
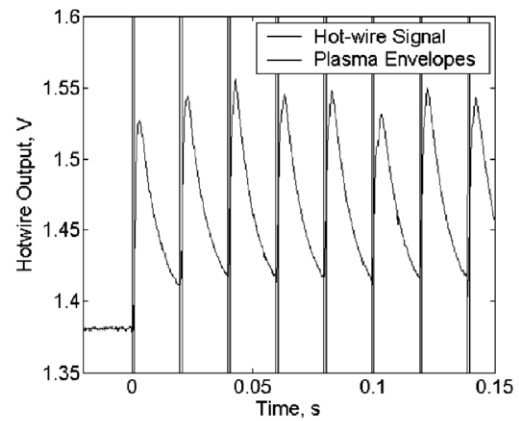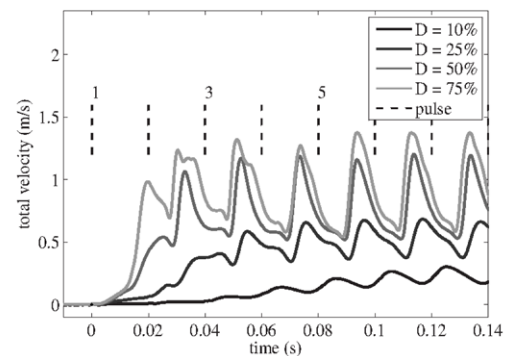
of individual particles is registered as they pass across the fringes. A spectrum analyser is then used to provide the light scattering frequency, which in combination with the known wavelength of the fringes can produce the velocity of the passing particle. By using pairs of laser beams at different wavelengths and different orientations, access to all velocity components at a given point is gained. Figure 6 shows the system used by Joussot *et al* [82].

LDV has excellent spatial and temporal resolution, ideally suited for plasma induced flows [64, 80, 85, 86]. The typical dimension of the interrogation volume (where fringes are developed) is in the order of tenths of millimetres [85]. As such, very high resolution of the developed flow field is possible. The same goes for temporal resolution with sampling rates as high as 10 kHz [64, 80]. In contrast to HWA, electrical arcing or EMI are non-issues here. In fact the application of LDV gave the first, undeniable evidence of the highly unsteady and periodic fluctuations of velocity in the plasma region [80].

On the other hand, LDV is a point measurement and, as such, able to resolve only one point in space per measurement. In order to resolve the entire flow field, the laser beams or the actuator must be traversed and measurements must be ensemble averaged in time [87]. Synchronised instantaneous information from multiple points in the flow domain is not
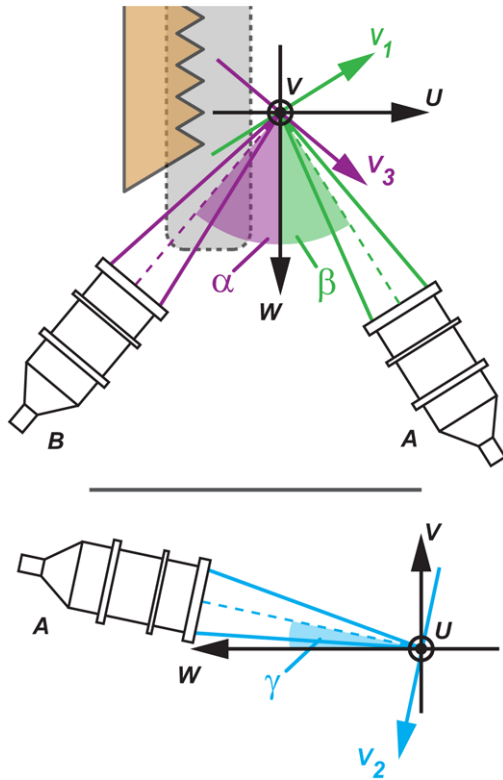
Figure 6. Three component laser Doppler velocimetry (3C-LDV) system used by Joussot *et al* [82]. Each velocity component (*u*, *v*, *w*) requires a laser beam pair of different wavelength. Reproduced with permission.

available. This can be somewhat mitigated by the strong periodicity of the unsteady plasma induced forcing. Based on this, phase ensemble average measurements [85, 87] can provide a global view of the actuator's dynamics.

The majority of LDV-based investigations on plasma actuators have made use of one- or two-component velocity measurements. Nevertheless, the easy expansion of the LDV technique into a three-component measurement (addition of a third beam pair and photodetector) provides a powerful method for characterising complex three-dimensional structures in the vicinity of atypical plasma actuators. Such a case was studied by Joussot *et al* [82] where serrated electrodes were used for inducing large span-wise coherent motion.

As a final note, care should be taken in LDV measurements regarding the introduction of tracer particles. If these are locally introduced in the vicinity of the actuator through a supply tube or orifice, it must be verified that such an approach does not interfere with the developed flow field. Alternatively, if the actuator is enclosed in an optical test chamber, it is recommended to fill the space with tracer particles of sufficiently homogenous distribution.

A second optical diagnostic technique in experimental fluid mechanics is PIV [89]. This is a field measurement technique, where velocity can be measured simultaneously in multiple points in the interest domain. As an evolution of LDV it relies on tracer particles inserted in the flow which are illuminated using fast laser pulses arranged in thin sheets. The position of the particles is registered using a digital imaging device,

usually a CCD or CMOS camera. By comparing two consecutive images separated by a known time interval, the velocity magnitude and direction of the flow can be simultaneously calculated in the entire imaged field. Depending on the configuration and specifications of the cameras and laser system, time-resolved measurements are possible at acquisition rates of few kHz.

Low repetition rate PIV has been extensively used for the characterisation of AC-DBD actuator induced velocity fields [70, 90–95]. The use of high resolution cameras, large magnification rate and well arranged optics can ensure high spatial resolution, necessary for plasma actuators. Typical vector densities of 2 [96] to 13 [97] vectors per mm have been reported. On the other hand, the size of the area of major acceleration and dynamics related to AC-DBD actuators is in the order of a few millimetres in the wall normal direction. The common issue with PIV near walls are light reflections, which contaminate the correlation process and degrade the resolving accuracy. Several solutions exist towards mitigating these effects such as aligning the laser sheet parallel to the surface, using non-reflective coatings, using advanced masking functions during processing and subtracting the ensemble average minimum intensity from the raw images dataset during preprocessing [98].

As a field velocity measurement, PIV has been a helpful tool in the study of AC-DBD actuators employing atypical geometric configurations such as annular and linear synthetic jets [91, 96, 99] or wedged-shaped and V-shaped electrodes [69].

High repetition rate, time resolved (TR-) PIV has been shown to be a useful tool in the investigation of the highly complex dynamics of the AC-DBD induced velocity [100, 101]. TR-PIV velocity measurements have provided reconstructions of the spatio-temporal evolution of the velocity field in the vicinity of the actuator (figure 8). These have been instrumental to the elucidation of the effects of the two HV half-cycles, and the importance of the shape of the applied waveform on the performance of the actuator [101] confirming previous time averaged observations [67].

Although most TR-PIV systems can achieve sampling rates up to 10 kHz, sufficient temporal resolution within the HV cycle would require additional effort. Phase locking techniques have been applied using both TR-PIV and PIV in order to increase the effective sampling resolution [82, 87, 100, 104–106]. The final acquisition dataset can be reconstructed into a higher resolution measurement than what the nominal sampling rate would allow. An important note here is the time separation between image pairs, which is usually in the order of microseconds. If this becomes too large, then measurement overlap between phases can reduce the effective sampling rate [100].

An important issue for both LDV and PIV techniques is the use of tracer particles [107]. Although under normal conditions these techniques can be considered non-intrusive, the existence of trace particles in areas of strong electric fields and ionisation typical for plasma actuators, should not be neglected (figure 9). Tracer particles can dissociate, get charged or magnetised due to the strong electric field. When charged, their movement is no longer governed purely by the
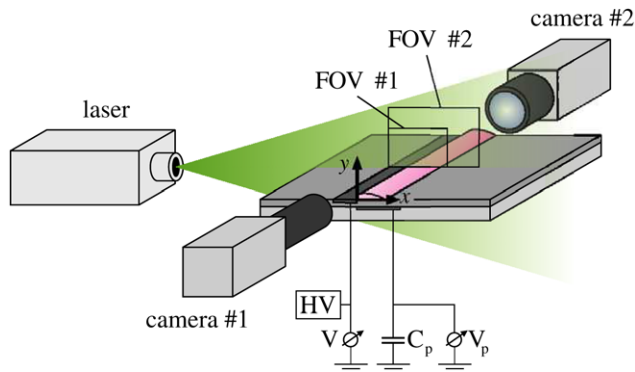
Figure 7. Two-component planar particle image velocimetry (2C-PIV) arrangement used by Kriegseis *et al* [88]. Two cameras were used to simultaneously image fields of view of different size. Reproduced with permission.
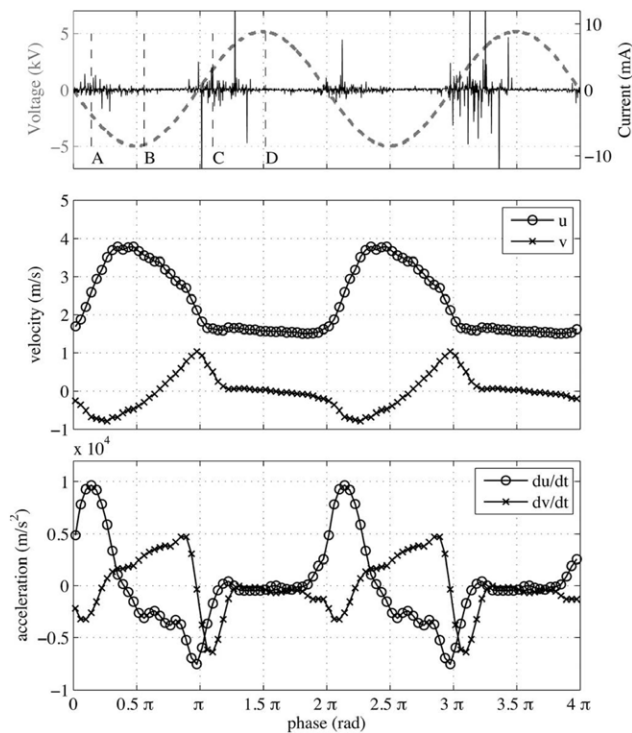

Figure 9. LDV measurements of induced velocity at two different positions downstream of the actuator (□: $x = 10.5$ mm, ○: $x = 20$ mm). Three different types of seeding materials have been used and results are compared with Pitot tube measurements of unseeded flow. Reproduced from [102] with permission.

Figure 8. Phase locked TR-PIV measurements of the unsteady velocity and acceleration in the vicinity of an AC-DBD actuator along synchronised measurements of voltage and current. Reproduced with permission from [100]. Copyright 2011, AIP Publishing LLC.

flow field but also by the electrical conditions [102]. An additional problem can be the accumulation of the tracer droplets on the wall which can influence the electrical properties of the dielectric [5].

Several studies have used Pitot tube measurements in seeded and non-seeded flow in an effort to quantify the effects of tracer particles on the measured velocities of AC-DBD actuators [102, 108–110]. Bousincha *et al* [102] investigated the effect of different materials such as olive oil, di-ethyl-hexyl-sebacat (DEHS) and incense smoke for tracer particles. They observed no significant effects on the shape of the velocity profile for these materials (figure 9). On the other hand the measured maximum velocity varied considerably between
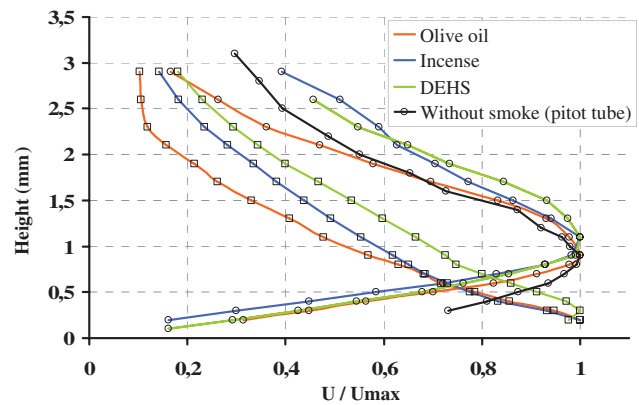
different materials and non-seeded flow. A recent study by Hamdi *et al* [103] made use of a needle-plane DC-corona configuration for testing several tracer particles. They observed considerable alterations of the voltage-current curve of the DC-corona between seeded and non-seeded flow depending on the tracer material. They conclude that incense smoke, titanium dioxide TiO_2 and silica SiO micro balloons are best suited for EHD flows. Of interest is the large charging effects they observe when using conductive oil material which is typical for commercial fog generation systems (disco smoke) used extensively by PIV laboratories (figure 10). This is a mixture of glycol, mineral oils and water. The results of Hamdi confirm the personal experience of the author in showing that disco smoke should be avoided for plasma actuator tests.

Additionally, some models have been devised in order to estimate whether the electrodynamic forces on tracer particles will be dominant compared to the hydrodynamic forces acting on the neutral gas [21]. Such models should be generally taken into account for the selection of seeding material for plasma actuator PIV testing. Finally, Masati *et al* [111] investigated the effect of the size of the tracer particles. Although they observed significant differences between cases, their results were inconclusive, stressing the need for further and more focused investigation into the charging effects.

A seedless visualisation technique that can be used for plasma actuators is Schlieren imaging. This technique is based on the optical detection of density gradients in the flow (a more detailed description of this technique is given in section 3). Some studies have employed Schlieren imaging in the visualisation of large induced structures from AC-DBD actuators [73, 113]. Unfortunately, due to the non-thermal nature of AC-DBD plasma the imaging intensity contrast is rather low allowing observation of only large coherent structures such as starting vortices. This can be partially improved by the addition of tracer gas of different density such as helium [112, 114] as shown in figure 11. In its conventional form this technique can provide only qualitative information for the flow. More advanced techniques such as Schlieren velocimetry are capable of some degree of quantitative information. However,
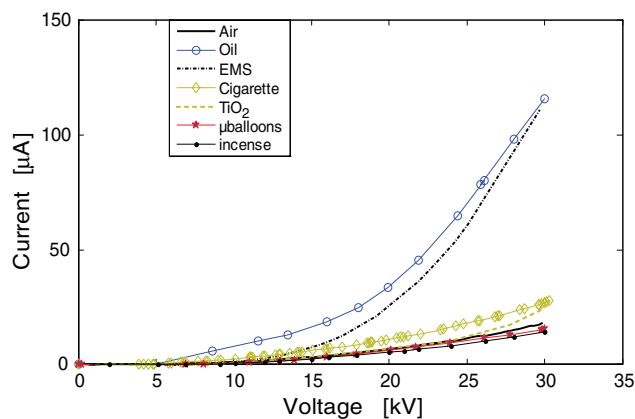
Figure 10. Voltage-current relation for a DC-corona discharge in the presence of several seeding materials. Note the large alteration of the curve in the case of conductive oil (disco smoke) and EMS compared to non-seeded (air) flow. Reproduced from [103] with kind permission from Springer Science and Business Media.

application to plasma actuators has received minimal attention [113, 114]. The spatial resolution of such an approach is rather insufficient for accurate description of the spatio-temporal dynamics of the AC-DBD actuator.

An alternative seedless visualisation technique has been demonstrated by Opaits *et al* [115]. This method is based on the rigorous production of ozone in the vicinity of the actuator due to recombination processes in the plasma cloud. A known property of ozone is its ability to absorb light in a very narrow band of 254 nm. An ozone visualisation technique based on this effect was first proposed by Dickerson and Stedman [116]. Opaits *et al* used a mercury lamp to illuminate the plasma volume near the actuator in a setup similar to Schlieren. They used a notch filter in order to capture only the 254 nm band. Due to the aforementioned absorption properties, areas of strong ozone generation appear as shadows in the captured images. Opaits *et al* used these in order to derive the ozone concentration due to the plasma actuator. Additionally they suggested that, in case of time resolved imaging, the visualisations could be correlated in a manner similar to PIV in order to derive velocity fields.

2.2. Body force

The flow control authority of AC-DBD plasma actuators is attributed to the creation of a volume-distributed body force of Coulombian origin [57]. This force is a product of collisions between heavy charged species (positive and negative ions) and neutral air particles. Several studies have attempted to measure the plasma produced force. Integral approaches involve either direct reaction force measurement based on balance and load cell readings or control volume momentum estimation techniques based on velocity fields. More advanced techniques use experimental flow field data, typically from PIV and Navier–Stokes based decompositions in order to derive the full spatial and temporal distribution of the body force. An overview of these efforts is given in table 2.

Measurement of plasma body force using the principle of reaction is the most popular and accessible technique due to the simplicity of the setup. Nevertheless, due to the extremely
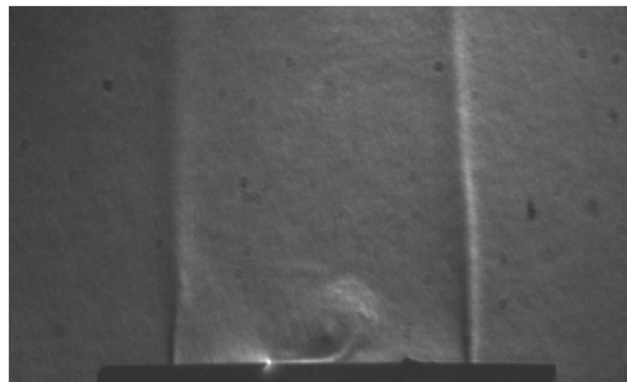

Figure 11. Schlieren imaging of a starting vortex due to AC-DBD actuation. The two vertical jets flanking the actuator are helium gas injections introduced in order to accentuate density and refractive index gradients [112]. Reproduced with permission.

small forces and the high voltages involved, accurate measurements are challenging. The concept relies on Newton's third law of motion stating that for every action there is an equal and opposite reaction. The AC-DBD actuator is able to accelerate flow in quiescent conditions as demonstrated by the formation of the wall parallel jet. By principle, the accelerated flow exerts an equal and opposite force on the actuator and its supporting structure. By supporting the actuator on a load sensitive device such as an electronic balance or load cell the spatially integrated plasma force can be measured.

Several studies have made use of off-the-shelf electronic balances [67, 118–122] or load cells [97, 101, 123]. Typical accuracy of such devises is in the order of 1 mg. The actuator assembly is either placed directly on the balance [67, 110] as shown in figure 12, or via a leveraged pendulum in order to amplify the measured force [118]. Special care should be taken due to the extremely small forces to be measured. The power and ground connections are usually made using thin copper electrodes or ball chains in order to avoid reaction forces from contaminating the measurement. Ashpis and Laun [124] review several practical methodologies towards acquiring consistent force measurements for AC-DBD actuators. As an alternative to electronic balances Porter *et al* [81] employed a technique based on the deflection of a pendulum for estimating the AC-DBD force.

A different technique for calculating the spatially integrated force of AC-DBD actuators has been the momentum balance analysis [81, 88, 97, 110, 120]. This is an implicit technique, which makes use of measured velocity profiles in the vicinity of the actuator. By applying a momentum integral in a control volume around the actuator, the space-integrated plasma force can be calculated. Velocity profiles acquired using Pitot tubes, LDV and PIV have been successfully used in this approach. The choice of the size of the control volume is quite important as has been shown by Durscher and Roy [110].

An important issue regarding reaction force measurements is the existence of the viscous friction force between the developed wall jet and the plate which is carrying the actuator. The skin friction force is always opposing the plasma actuator body force, thus resulting in an underestimation of the latter. It is then expected that the physical size of the flat plate

Table 2. Overview of body force measurement works.

Steady measurements				
Reference	Technique	Voltage (p–p) [kV]	Frequency [kHz]	Notes
Enloe *et al* (2004) [118]	reaction scale	4–16	3–6	waveform study
van Dyken *et al* (2004) [119]	reaction scale	2–12	5	parametric study
Porter *et al* (2007) [81]	momentum balance (Pitot), hanging pendulum, accelerometer	10–20	5–20	comparison of techniques
Abe *et al* (2008) [126]	reaction scale	12–20	1–5	parametric study
Hoskinson *et al* (2008) [120]	reaction scale, momentum balance (Pitot)	12–26	0.5–1	comparison of techniques
Porter *et al* (2009) [69]	momentum balance (Pitot)	19	5–10	non-linear actuators
Thomas *et al* (2009) [67]	reaction scale	5–75	1–8	thick dielectrics
Wilke (2009) [132]	velocity field	14	0.8–1	force field estimation
Albrecht *et al* (2011) [136]	velocity field	—	—	Lorentz force
Cheong *et al* (2011) [121]	reaction scale	13–16	13–16	angular actuators
Kriegseis *et al* [122]	reaction scale	10–25	8–13	
Kotsonis *et al* (2011) [97]	velocity field	8–16	1–4	force field estimation
Durscher and Roy (2012) [110]	reaction scale, velocity field	14–28	7–14	comparison of techniques
Kotsonis and Ghaemi (2012) [101]	reaction scale	20–40	0.6–1	asymmetric waveform
Kriegseis *et al* (2013) [88]	velocity field	8–12	11	comparison of techniques

| Unsteady measurements				
Reference	Technique	Voltage (p–p) [kV]	Frequency [kHz]	Notes
Enloe *et al* (2008) [127]	hanging pendulum	30	0.065	use of interferometry
Font *et al* (2011) [128]	torsional pendulum	14–30	0.2	effect of oxygen
Debien *et al* (2012) [104]	momentum balance (PIV)	40	1	
Benard *et al* (2013) [135]	velocity field	40	1	spatio-temporal force
Elias and Castera (2013) [129]	interferometry	20	0.4	impulse of ns-DBD
Murphy *et al* [106]	velocity field	7–13	2–4	spatio-temporal force
Neumann *et al* (2013) [87]	velocity field	6.4	9.5	comparison of techniques
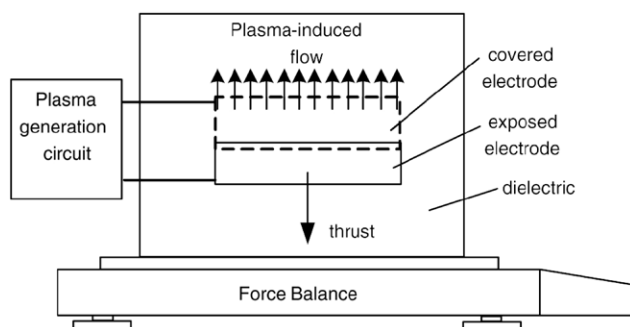
Figure 12. Reaction force balance setup used by Thomas *et al*. From [67]; reprinted by permission of the American Institution of Aeronautics and Astronautics, Inc.

downstream of the actuator affects the measured force. Indeed Durscher and Roy [110] demonstrated that the measured force could increase as much as 20% when shortening the flat plate from 15 to 2.5 cm. Furthermore a recent study by Pereira *et al* [123] showed that the body force can be underestimated by as much as 50% due to friction forces.

Similar to reaction force measurements, the consideration of the friction force is important for control volume approaches. Some works [88, 125] have directly calculated this using the measured velocity data and the shear stress definition:

$$\tau = \frac{\partial u}{\partial y}\bigg|_{y=0} \tag{2}$$

where τ is the shear stress at the wall. Others have considered it part of the measured force [97, 101]. A second note is the existence of the pressure gradient term. This cannot be readily resolved using the velocity measurements due to the existence of the plasma force. On the other hand, if the control volume is
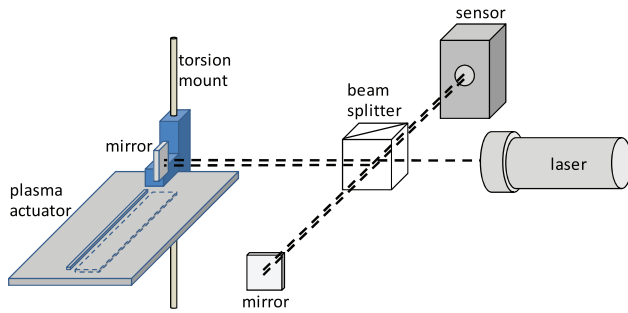
Figure 13. Torsional pendulum setup used by Font *et al* [128] for unsteady force measurements of AC-DBD actuators. The displacement of the actuator-carrying plate is measured using interferometry. Reproduced with permission.

selected to be such that its boundaries do not cross regions of significant pressure gradients, then its net effect can be incorporated into the value of the measured body force [110].

Measurements of time- and space-averaged force are important for extensive parametric studies [67, 126]. On the other hand, the insight into the underlying physics governing the operation of the actuator is often limited due to the lack of time resolved information and spatial topological features of the produced body force. Several techniques have been proposed to gain access to the time-resolved forcing behaviour of the actuator.

Porter *et al* [81] used a calibrated accelerometer attached directly to the actuator in order to access the time resolved evolution of the force. They carefully used a circular actuator as to have the force impulse arrive at the accelerometer simultaneously from the entire actuator. Enloe *et al* [127] used the same setup but a different technique for measuring the force. They employed a Michaelson interferometer measuring the resonant oscillation of the pendulum carrying the actuator. The Michaelson interferometer approach has also been used by Font *et al* [128] on a torsional pendulum (figure 13). It must be noted that theses studies relied on the calibration of the results with theoretically predicted resonance based on vibration analysis of the pendulum system. They verified earlier velocity-based observations [92] regarding the dominance of the forward stroke and negative ions in the momentum production budget. In fact they showed that both half cycles produce positive forces (Push–push scenario[3]).

In a rare force measurement study for ns-DBD actuators, Elias and Castera [129] used an interferometer to measure the impulse imparted on the flow by a ns-DBD actuator. By integrating the impulse with the pulse frequency they produced the average thrust due to ns-DBD actuation. This is perpendicular to the dielectric surface and its origin is the intense local heating and expansion of gas in contrast to the ionic wind associated with AC-DBD or DC-corona actuators.

Debien *et al* [104, 130] have made use of momentum balance analysis on time resolved velocity measurements in order to derive the time resolved plasma force. Their integral analysis was based on the approach of Noca *et al* [131]. They

---

[3] For the entirety of this review paper the definition of forcing scenarios is the one introduced by Corke [2]. The two events correspond to the negative and positive half cycle of applied voltage respectively, while the dominant action is denoted by a capital letter.

showed time resolved evolution of the force for both plate and wire exposed electrodes. In contrast to the previously mentioned direct force measurements [81, 127, 128] they showed negative force for the backward stroke resulting in a Push–pull scenario (figure 14). On the other hand, Murphy *et al* [106], using the momentum balance technique of Versailles *et al* [125], showed a positive force throughout the cycle (Push–push) even at instants were plasma is not ignited. The discrepancies between the different studies highlight the importance of effects such as local pressure gradients and viscous forces on force estimation using velocity data.

The spatial and full spatio-temporal distribution of the AC-DBD body force has also received considerable attention. Several approaches have been proposed towards decomposing velocity field measurements (usually form PIV) using the Navier–Stokes (NS) equations (figure 15). The 2D incompressible NS equations in the presence of body forces (*F*) read as:

$$\frac{\partial U}{\partial t} + U \cdot \nabla U - \nu \nabla^2 U = -\frac{\nabla p}{\rho} + \frac{F}{\rho} \qquad (3)$$

where *U* is the 2D velocity field, *p* is the static pressure, ν is the kinematic viscosity of the fluid and ρ is the density.

All the velocity terms of the NS equations are readily available from field measurements such as time-resolved or phase-averaged PIV. On the other hand, the pressure term cannot be explicitly resolved when body forces exist. Several techniques have been applied in the field of experimental aerodynamics for the estimation of the pressure term from velocity data [133]. The majority of these techniques assume negligible body forces as they treat more classical problems such as flow around airfoils [134]. This is certainly not the case with the plasma actuator as body forces coexist with localised pressure gradients. Therefore, an inherent problem in separating the body force and pressure gradient term exists that has received considerable attention.

Wilke [132] and later Kriegseis *et al* [88] and Neumann *et al* [87] assumed that the pressure gradient is significantly smaller than the body force and neglected it altogether. They have then used a CFD simulation inserting the experimentally derived force distribution in a quiescent flow domain. By comparing the computed wall jet with the original experimental data they concluded that their initial assumption was valid. In contrast, the term decomposition technique by Kotsonis *et al* [97] showed that the pressure gradient term is far from negligible and in the same order of magnitude as the body force, especially very near the actuator (figure 16). The source of this discrepancy lies in the workings of incompressible CFD solvers. Since pressure does not have an independent equation it must be iteratively computed using the last known velocity field (e.g. SIMPLE algorithm [137]). In the case that the source term is a combination of a body force and a (non-negligible) pressure gradient such as the one that is measured by PIV, then the solver will produce an *apparently correct* flow field without the need of imposing any pressure gradient, leading to a false assumption.

Albrecht *et al* [136] arranged the NS equations using the velocity–vorticity formulation, thus eliminating the pressure term. They then assumed that the remaining curl of the body force can be solved by neglecting the gradient
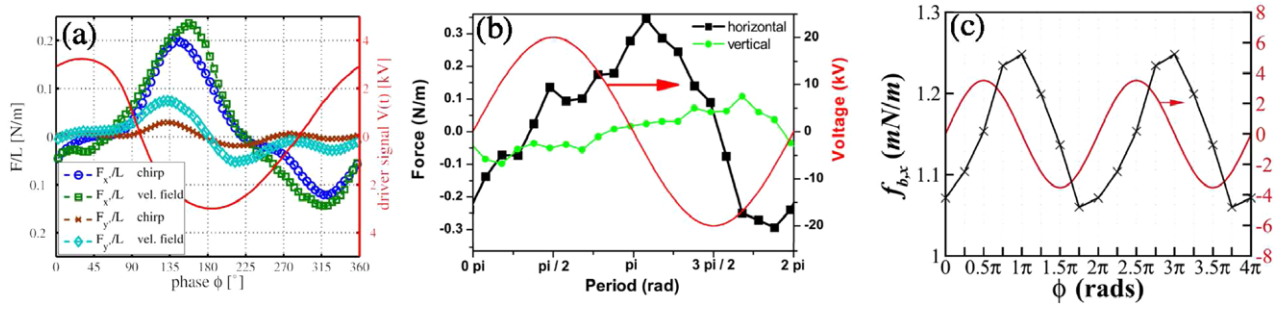
Figure 14. Temporal evolution of body force calculated from velocity measurements. (a) LDV measurements of Neuman *et al* [87] (reproduced with permission) using the method of Wilke [132], (b) PIV measurements of Debien *et al* (Reproduced with permission from [104, 130]. Copyright 2012, AIP Publishing LLC.) using the method of Noca *et al* [131], (c) PIV measurements of Murphy *et al* (Reproduced with permission from [106]. Copyright 2013, AIP Publishing LLC.) using the method of Versailles *et al* [125].
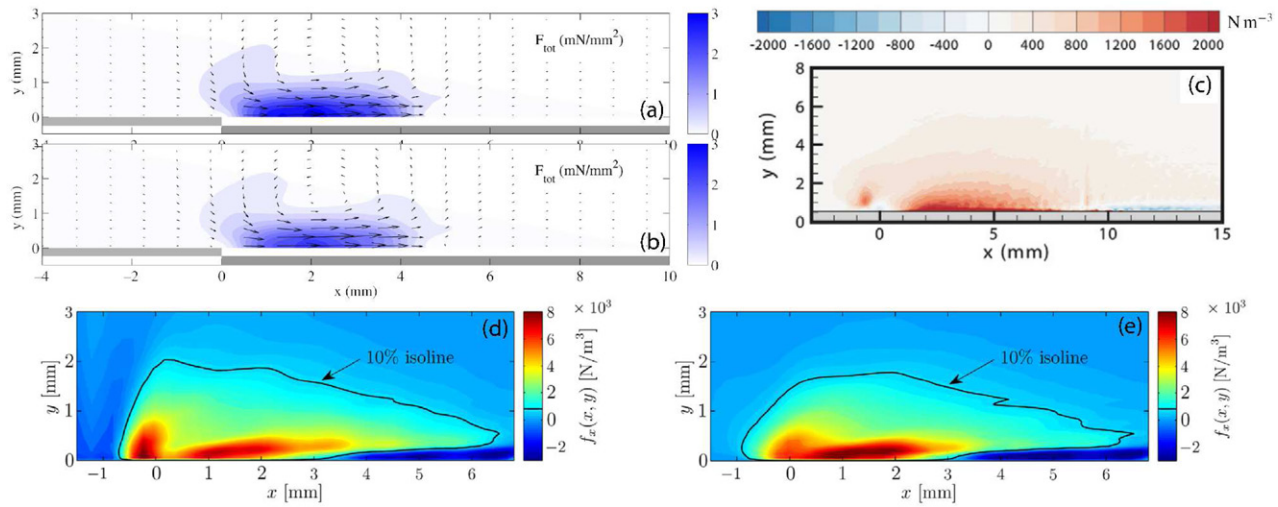

Figure 15. Spatial distribution of AC-DBD actuator body force from velocity data using different techniques; (a) and (b) results of Kotsonis *et al* using own method. Reproduced from [97]. (c) Results of Benard *et al* [135] and (d) Kriegseis *et al* [88] using the method of Wilke [132]. Reproduced with permission. (e) Results of Kriegseis *et al* [88] using the method of Albrecht *et al* [136]. Reproduced with permission.
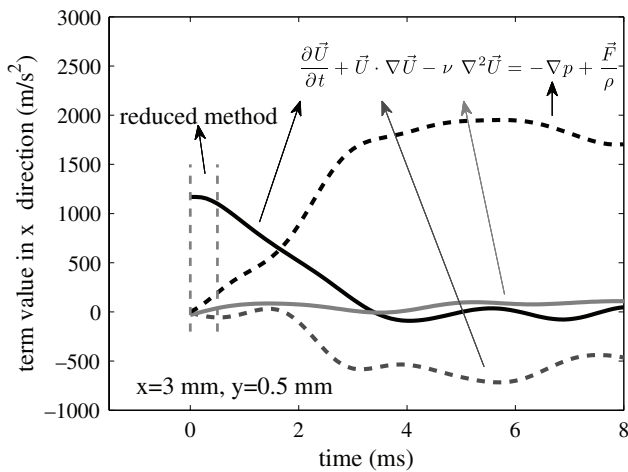

Figure 16. The term decomposition of the Navier–Stokes equations using the method of Kotsonis *et al* [97]. Note the dominance of the acceleration term in the *reduced method* and the pressure gradient and convective terms in the *gradient method*. Reproduced with permission.

of the wall normal component ($\partial f_y/\partial x$) and through integration they arrived at the force in wall parallel direction (f_x). Good agreement of their results was established with PIV measurements on a Lorentz force actuator in locations

far from the actuator. In regions where f_y was large their method failed.

Kotsonis *et al* [97] made use of time-resolved PIV measurements of an impulsively started AC-DBD actuator. They developed two techniques. For their *reduced method* they assumed that for the very first moments after the impulsive start of actuation, acceleration is the only dominant term thus directly equal to the body force. For their *gradient method*, they assumed that the plasma body force is steady in the time scales of the transient development of the induced jet (order of tens of milliseconds). Based on this they differentiated the NS in time, thus eliminating the force term. By assuming a zero pressure gradient prior to actuation, they were able to back-calculate the pressure gradient term and eventually the body force. Although good agreement of this method was established with reaction force measurements, by nature of assumptions the time resolved force within the HV cycle cannot be calculated with this method.

Finally, full spatio-temporal evolutions of the AC-DBD plasma body force have been estimated using the method of Wilke [132] by Neumann *et al* [87] using phase-averaged LDV measurements and Benard *et al* [135] using low repetition phase-averaged PIV measurements. Both studies showed that the assumption of negligible pressure gradient can provide a

first order qualitative approximation to the plasma body force. On the other hand the procedure of Benard *et al* [135] produced negative forces at time instants in which plasma was not present, which can suggest that the pressure gradient indeed has an important role to play in this process. This is further supported by the time-resolved density measurements of Enloe *et al* [138] as well as the NS terms decomposition of Kotsonis *et al* [97].

3. Thermal characterisation

Thermal effects attributed to the operation of plasma actuators have been treated in a number of studies. A group of investigations involves the release of heat from prolonged operation of AC-DBD actuators. Although the developed temperatures do not reach extreme levels, the identification of the thermal loading of the dielectric material and supporting structures is of importance for future applications. Additionally, the ionised species and surrounding gas temperature can give considerable insight into the discharge process. Thermography techniques based on infrared imaging (IR), cold wire anemometry (CWA) and optical emission spectrography (OES) have been applied.

A second group of investigations is devoted to thermal effects as flow control mechanisms. This is particularly important for a sub-category of plasma actuators based on repetitive nanosecond pulses in place of the more conventional AC voltage. For the ns-DBD actuators thermal effects dominate body force and momentum effects. Several investigations based on density gradient detection such as Schlieren imaging, shadowgraphy and interferometry have been conducted. An overview of thermal characterisation studies for both kinds of plasma actuators is presented in table 3.

3.1. Thermal characterisation of AC-DBD actuators

A variation of the HWA technique aimed at measuring temperatures is cold wire anemometry (CWA). It employs the same thin wire sensors as with HWA, albeit using a different operation principle. The electronic bridge is configured as to keep the current flowing through the thin wire constant. Under these conditions the wire is relatively insensitive to flow variations but the bridge voltage is linearly proportional to the temperature of the flow. CWA combines high sampling rates with sufficient accuracy. Careful calibration is essential and possible ambient temperature drifts must be taken into account.

Jukes *et al* [76, 79] made use of the CWA technique in order to measure temperature of the induced flow of an AC-DBD actuator (figure 17). They registered very weak increase of the flow temperature, in the order of 2 °C demonstrating the non-thermal nature of this type of discharge. Similar to HWA studies, problems of EMI and arcing between the plasma and the wire were encountered.

Due to proximity issues and losses in cases where the CWA sensor is very near the wall, Jukes *et al* [76] measured at wall normal distances larger than one millimetre. Additionally, their results indicated strong diffusion effects, responsible for the weak gas temperature increase several millimetres from the actuator. The thermal deposition directly inside the plasma region can be
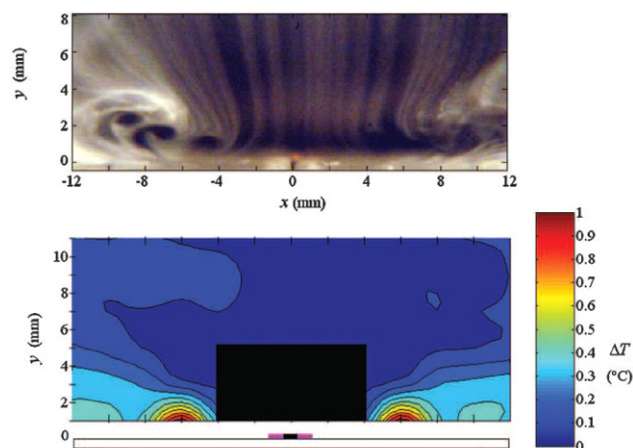

Figure 17. Cold wire anemometry (CWA) measurements of the flow temperature in the vicinity of an AC-DBD actuator. The smoke visualisation reveals the induced flow topology. Reproduced by permission of SAGE Publications Ltd., London, Los Angeles, New Delhi, Singapore and Washington DC, from [79], Copyright (© SAGE, 2008).

considerable, with respective effects on the dielectric surface and gas temperature. A technique that can provide quantitative measurements of the surface temperature is infrared thermography [79, 139–142]. This method is based on direct imaging of heated bodies with specialised thermographic cameras detecting light in the infrared spectrum (figure 18). Joussot *et al* [141] verified dielectric surface temperatures of up to 60 °C in the immediate vicinity of the plasma region for quiescent conditions. The temperature decreased rapidly with increasing distance from the actuator and reached ambient levels within 20 mm. Additionally, they performed these measurements under conditions of external flow and demonstrated a significantly weaker temperature increase attributed to forced convection. It should also be noted that surface temperature is a strong function of the dielectric material properties (thermal capacitance and conductivity).

A more recent study from Tirumala *et al* [139] applied the thermographic technique analysis in combination with light emission measurements using an intensified CCD camera. They found strong spatial correlation of the surface temperature with the discharge. More specifically, the high temperature spots were aligned to the glow spots corresponding to areas of electric streamers. Additionally strong morphological variations of both the discharge and the thermal footprint were observed for different applied voltage waveforms.

Experimental emission spectrography is a common technique applied in various areas of applied and fundamental physics in order to gain information on the spectral content of electromagnetic emissions [143]. This is a powerful technique in the field of plasma actuators due to the multitude of information it can give access to, otherwise unattainable through classic flow diagnostics [144–147]. A typical spectrographic setup would include an optical system positioned above the discharge area. This is responsible for the detection and collimation of the emitted radiation. The detected signal is then sent to a monochromator via optic fibers, in order to select the spectral band of interest using either prisms or diffraction gratings. Finally, the selected band is registered using a digital camera.

Table 3. Overview of thermal characterisation studies.

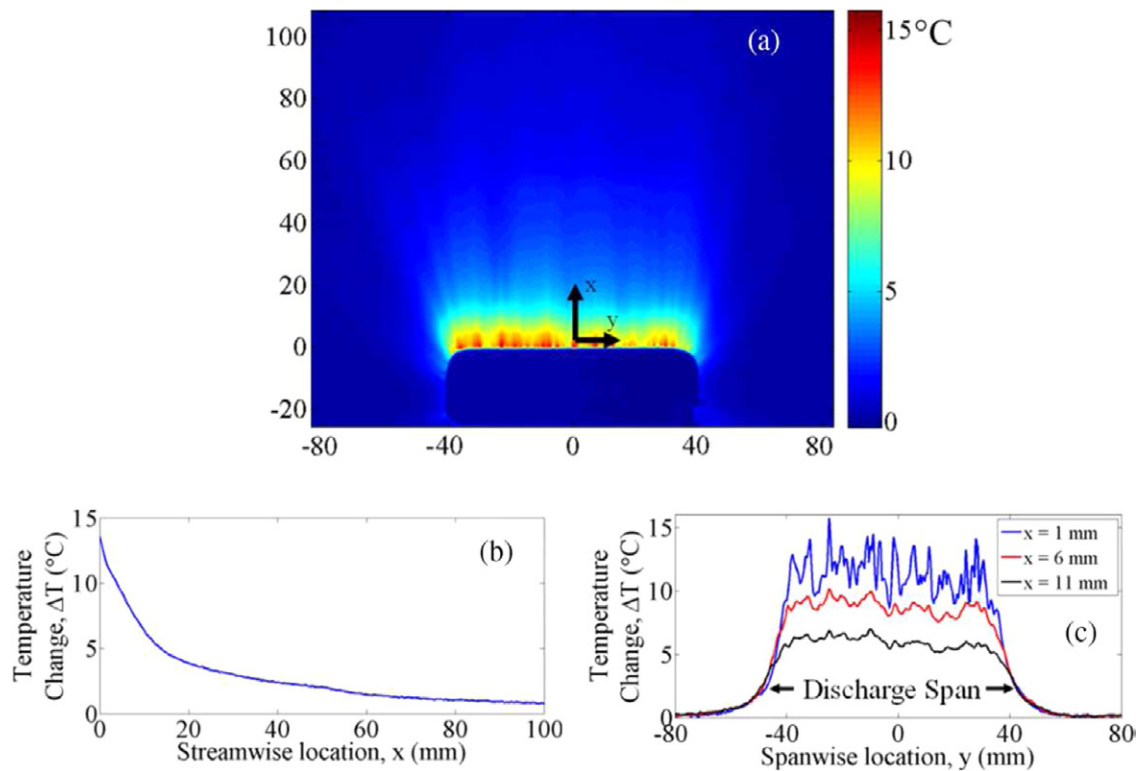| AC-DBD actuators				
Reference	Technique	Voltage (p–p) [kV]	Frequency [kHz]	Notes
Jukes *et al* (2006) [76]	CCA	8	50	
Dong *et al* (2008) [63]	spectrography	10–20	1	array of plasma actuators
Joussot *et al* (2010) [141]	thermography	8–30	1	parametric study
Neretti *et al* (2012) [142]	thermography, spectrography	10–55	10–28	effect of dielectric thickness
Tirumala *et al* (2014) [139]	thermography	21–38	0.2–1.5	parametric study
ns-DBD actuators				
Reference	Technique	Voltage (p–p) [kV]	Frequency [kHz]	Notes
Opaits *et al* (2008) [149]	Schlieren	10	3	with DC-bias
Starikovkii *et al* (2009) [40]	laser Schlieren	12–24	single pulse	
Benard *et al* (2012) [150]	Schlieren	10	single pulse	effect of pulse width
Dawson and Little (2013) [151]	Schlieren	10	1	effect of actuator length
Elias and Castera (2013) [129]	Schlieren	20	single pulse	
Correale *et al* (2014) [152]	Schlieren	12	10	bursts of 10, 20 and 50 pulses

Figure 18. (a) Infrared thermography measurements of the surface temperature in the vicinity of an AC-DBD actuator, (b) change in temperature in streamwise and (c) spanwise directions. The change in temperature is measured after a 4 minute period of operation [139]. Reproduced with permission.

The measured spectra intensities accessed through spectrography need elaborate processing depending on the physical quantities which are required to be resolved. In atmospheric pressure conditions the most dominant feature in the spectra of air is the second positive system (SPS) of molecular nitrogen [63, 146]. The peak intensity of the SPS can provide the vibrational temperature through a semi-log Boltzmann plot of energy versus intensity [142]. The fit quality of the measured peaks on the Boltzmann plots can also assure the validity of the Boltzmann distribution assumption.

To access translational and rotational temperatures, measured spectra are usually compared with numerical predictions of commercial packages such as SPECAIR [148]. Once the measured spectra fit the model predictions, temperatures can be retrieved directly from the model (figure 19).

The translational and rotational temperatures are approximately equal to the gas temperature in atmospheric pressure [147]. This has been demonstrated by comparing with thermographic measurements of the dielectric surface directly below the plasma region [142]. In contrast, vibrational temperatures
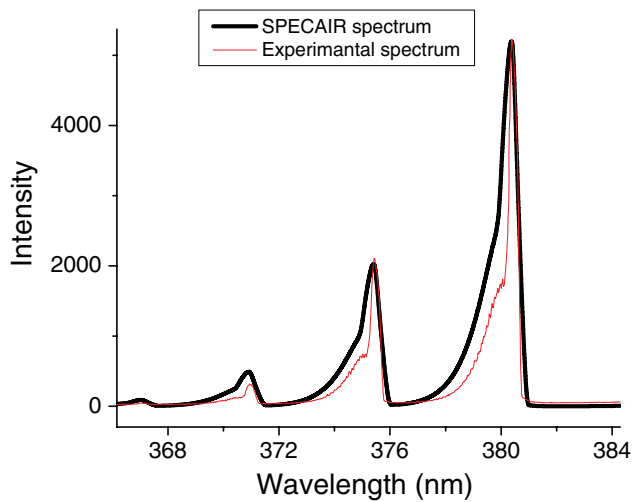
Figure 19. Measured spectrum of the second positive system of nitrogen in atmospheric air DBD plasma actuator with the corresponding theoretical fit from SPECAIR. Reproduced from [145].

have been observed to be one order of magnitude higher and relatively independent of test conditions [142].

3.2. Thermal characterisation of ns-DBD actuators

Nanosecond-pulsed DBD actuators have received considerable interest due to their apparently superior control authority over the AC-DBD in the specific case of control of leading edge separation [45]. While their material and geometric features are indistinguishable from conventional AC-DBD actuators, ns-DBDs have an entirely different working principle. The core of their operation relies on the use of repetitive HV pulses of width ranging from tens of nanoseconds [40, 152] to tens of microseconds [150]. The rapid increase of voltage results in molecular dissociation and fast recombination of charged species. The latter is responsible for fast thermalisation (i.e increase in temperature) of the plasma layer and, in consequence, rapid heating of the neutral gas near the surface of the actuator. Due to the thermal expansion a weak pressure wave is produced which starts propagating at near-sonic velocities [40, 151, 152].

The ns-DBD is thus identified by two main features, which eventually define the ideal measurement technique for its thermal characterisation. These are the area of intense gas thermalisation near the actuator (*hot spot*) and the compression waves following each pulse. Both of these phenomena are accompanied by pronounced density gradients. A typical technique able to quantify changes in density that has been used in the field of compressible aerodynamics for the past one and half century is Schlieren imaging. In fact one of the first applications of Schlieren imaging was the observation of the electric wind in corona discharges [13]. This is an optical technique based on refraction index differences of the measured medium. These are directly related to density gradients. When light is directed throughout the density gradients of the medium it deflects compared to light passing from optically uniform areas. By using a knife edge the undeflected light is partially blocked. The deflected light then creates highlights

or shadows in an imaging plane, depending on the direction of the density gradient. The imaging plane is typically recorded using a digital camera. By using fast stroboscopic lights, rapid events can be frozen in time in order to reveal the instantaneous structures. A typical Schlieren imaging arrangement is shown in figure 20. It should be noted here that no explicit temperature information can be derived from Schlieren imaging. Nevertheless, due to the inherent thermal nature of ns-DBD actuation, we have classified Schlieren imaging as a thermal characterisation technique.

Compression waves are produced at each pulse during actuation of ns-DBD [40, 153] (figure 21). The propagation velocity of the waves is approximately sonic in lab atmospheric air conditions [129, 152]. Regarding the shape of the compression waves, Dawson and Little [151] aligned their Schlieren setup in order to measure in both the stream wise and span wise planes. They showed that the apparent cylindrical compression wave is actually composed of several spherical waves emanating from local discharge non-uniformities along the span of the actuator. These propagate away from the actuator with a common front. Benard *et al* [150] demonstrated that in fact two pressure waves are present for each pulse. By using pulse widths of up to several microseconds they observed one compression wave during voltage rise and one during voltage drop. Naturally, the two waves are almost superimposed for short nanosecond pulses.

Opaits *et al* [149] used the Schlieren technique with a non-typical actuation scheme where the nanosecond pulses were superimposed on a sinusoidal or DC voltage. The localised heating due to the pulse allowed the visualisation of the starting vortices formed by the low frequency sinusoidal voltage.

Still based on diffraction gradients but using a different technique, Pons *et al* [154] measured the compression waves with a Mach–Zehnder interferometer (figure 22). This is a technique based on measuring the phase shift between two coherent light beams. The coherency of the beams is ensured by splitting a single laser beam. One of the two beams is passed through the medium to be measured while the other is passed through uniform medium. The beams are then recombined and a fringe pattern is formed. The deformations of the fringes reveal density gradients and can be registered using a digital camera. Pons *et al* [154] used this technique for linear and serrated electrodes demonstrating that the wavefront of the compression wave is indeed the superposition of individual spherical waves.

Correale *et al* [152] extended the Schlieren measurement observation time for several milliseconds after the application of the pulse. They observed the formation of strong thermalised gas areas (*hot spots*) in the vicinity of the actuator long after the compression wave was emitted (figure 23). By imaging of the spanwise plane, they found pronounced non-uniformities of the hot spot correlating with areas of strong discharge filaments. This study challenged the common perception regarding the flow control mechanism of ns-DBD actuators. While earlier studies [40] suggested that the actuator was perturbing the flow via the compression wave, Correale *et al* [152] argue that strong density and/or viscosity gradients might play an equal or stronger role.

In principle, spectroscopy can be used for ns-DBD actuators for accessing the gas temperature in the vicinity of the
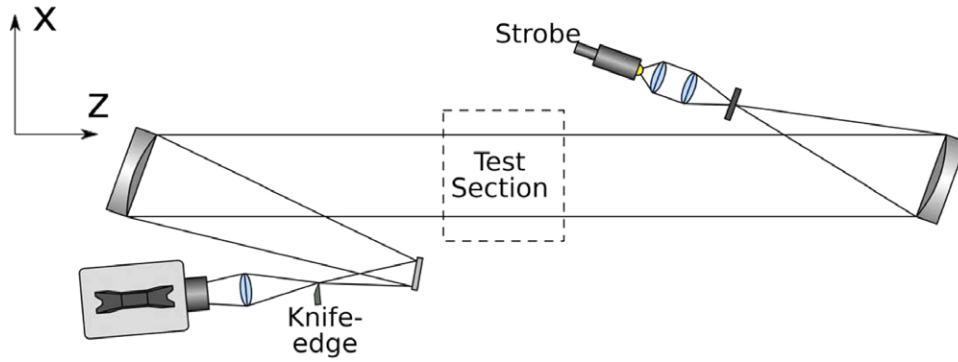
Figure 20. Schlieren imaging arrangement used by Correale *et al* for the characterisation of ns-DBD actuators. Reproduced from [152].
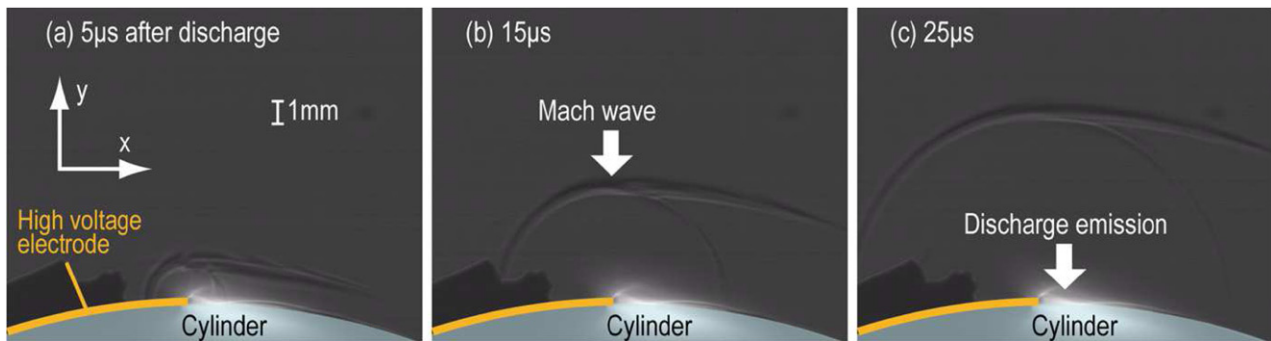

Figure 21. Schlieren imaging of weak compression waves due to single nanosecond pulse at different elapsed times from actuation. Reproduced from [153].
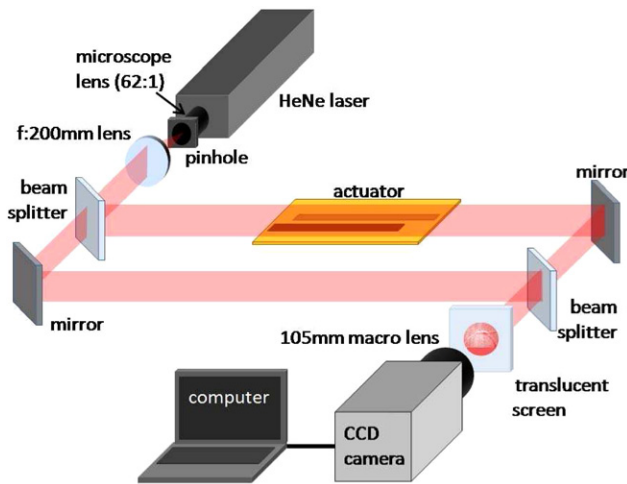

Figure 22. Mach–Zehnder interferometry setup used by Pons *et al* for the detection of density gradients due to ns-DBD actuation. © 2014 IEEE. Reprinted, with permission, from [154].

Figure 23. Schlieren imaging of ns-DBD actuation after 50 repetitive pulses at frequency of 10 kHz. A strong thermal area (*hot spot*) is formed and sustained long after the last compression wave is emitted. Reproduced from [152].

actuator. To date only Starikovskii *et al* [40] and Takashima *et al* [153] have obtained spectroscopic measurements of ns-DBD actuators. Both studies showed an increase of gas temperature of almost 100 °C depending on input energy.

4. Electrical characterisation

Plasma actuators are powered using high voltage, high frequency signals. In addition, the plasma formation in itself is a highly dynamic process dominated by a strongly multi-scale

behaviour. Applied voltage periods are in the order of milliseconds while several plasma formation or destruction processes are taking place in micro- or nanoseconds [155].

These features complicate the electrical characterisation of these devices. Power measurements require synchronised measurements of both applied voltage and discharge current. Especially the latter is dominated by high frequency, high amplitude spikes which complicate its measurement.

Table 4. Overview of electrical characterisation works.

Reference	Technique	Voltage (p–p) [kV]	Frequency [kHz]	Notes
Enloe *et al* (2004) [118, 156]	shunt resistor, PMT	4–16	3–6	waveform study
Pons *et al* (2005) [68]	shunt resistor, shunt capacitor	20–60	0.3–1	
Sasoh *et al* (2007) [157]	shunt resistor, iCCD	2–10	1–5	fast imaging
Dong *et al* (2008) [63]	Rogowski coil, shunt capacitor, spectrography	10–20	1	array of plasma actuators
Moreau *et al* (2008) [112]	shunt resistor	40	1	sliding discharge
Opaits *et al* (2008) [158]	electrostatic voltmeter probe	10	3	with DC-bias
Dedrick *et al* (2010) [144]	Rogowski coil, spectrography	2.4	13.56 MHz	RF power
Leonov *et al* (2010) [75]	iCCD	24	0.02–2	in air and nitrogen
Font *et al* (2011) [128]	V-dot probe	14–30	0.2	
Gulec *et al* (2011) [145]	iCCD, spectrography	24	1	
Giepman and Kotsonis (2011) [159]	shunt resistor	8–16	1–4	efficiency study
Joussot *et al* (2011) [160]	iCCD, Rogowski coil	36	1	
Takashima *et al* (2011) [153]	shunt resistor, iCCD, spectrography	17	0.01–1	ns-DBD
Cristofolini *et al* (2012) [113]	Hall sensor	20–35	5	
Kriegseis *et al* (2011) [122, 161]	shunt capacitor, CMOS camera	6.5–12.5	8–13	detailed parametric study
Ashpis *et al* (2012) [162]	shunt resistor, shunt capacitor	8	2	power measurement
Benard and Moreau (2012) [86]	shunt resistor, shunt capacitor, iCCD	40	1	effect of waveform
Benard *et al* (2012) [150]	Rogowski coil, iCCD	10	single pulse	ns-DBD
Debien *et al* (2012) [105]	shunt resistor, shunt capacitor, iCCD	28–44	1–1.5	wire electrodes
Aba'a Ndong *et al* (2013) [163]	Rogowski coil, iCCD	10	1 pulse	ns-DBD
Biganzoli *et al* (2013) [146]	Rogowski coil, shunt capacitor, spectrography	24–50	10–30	
Cristofolini *et al* (2013) [164, 165]	Hall sensor, electrostatic voltmeter probe	15–30	5	
Dedrick *et al* (2013) [95]	Rogowski coil	7	5	13.5 MHz pulses
Elias and Castera (2013) [129]	Rogowski coil, iCCD	20	single pulse	ns-DBD
Jiang *et al* (2013) [166]	Rogowski coil	18	single pulse	ns-DBD
Joussot *et al* (2013) [82]	shunt resistor, shunt capacitor, iCCD	4–38	1	serrated electrodes
Stanfield and Menart (2013) [147]	spectrography	11.6	5	
Nichols and Rovey (2013) [167]	V-dot probe	13.4	5	AC-DBD
Correale *et al* (2014) [152]	shunt resistor	12	10	ns-DBD
Neretti *et al* (2014) [73]	Hall sensor	3.4–6	15	vectorised actuator
Pang *et al* (2014) [168]	Rogowski coil	3–19	single pulse	ns-DBD
Pons *et al* (2014) [154]	Rogowski coil, iCCD	15	single pulse	atypical ns-DBD

The morphology and formation of the discharge is also of importance towards better understanding of the fundamental operating principles of the plasma actuator. The strong asymmetry between the two half cycles in AC-DBD actuators results into different discharge regimes which can be visualised using fast optical imaging. Additionally, optical emission spectroscopy can provide further information regarding the density of charge, electrical field and charge accumulation. An overview of electrical characterisation studies is shown in table 4. It must be noted here that the electrical characterisation studies covered in this paper are solely concerned with plasma actuators. A vast number of studies can be found for the more general cases of surface or volume DBDs or other types of plasma discharge. Similar techniques as the ones described here, such as optical emission spectroscopy, electrostatic probes and fast imaging, have been a staple for the characterisation of cold plasmas. The coverage of these works is beyond the scope of this paper.

4.1. Voltage, current and power of AC-DBD actuators

Measurement of the applied voltage for AC-DBD and DC-corona actuators is relatively straightforward. Most commercial power supplies or high voltage amplifiers provide functionality for monitoring the output, usually via a scaled-down voltage signal. In case this option is not available, the
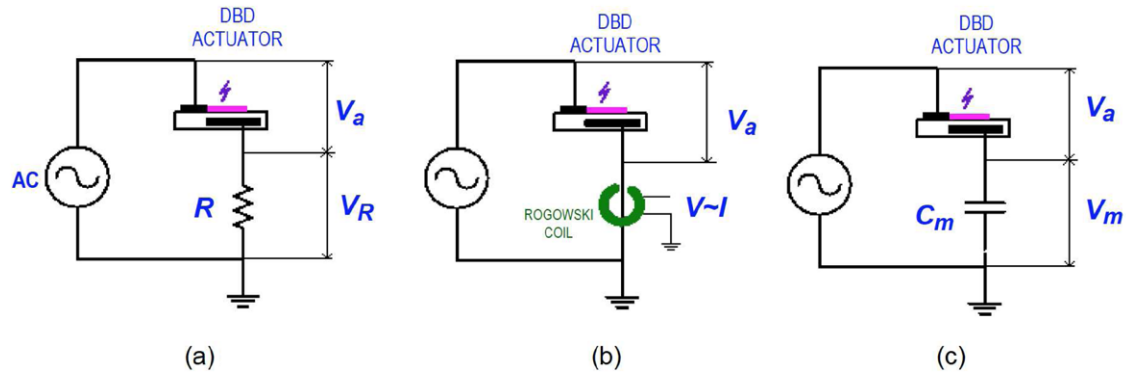
Figure 24. Typical arrangements for current and power measurements for plasma actuators. (a) Shunt resistor technique, (b) induction based technique, (c) shunt capacitor technique. From [162]; reprinted by permission of the American Institute of Aeronautics and Astronautics, Inc.

powered electrode can be directly connected to a fast high voltage probe. The output of the power supply or HV probe can be read using a fast oscilloscope or data acquisition system (DAQ). Small differences can appear between direct voltage measurements on the electrode using HV probes and local output using the built-in monitor of the power supplies. These are due to the extra length of the HV cable (usually a few meters) and the associated increase in impedance [162].

Accurate measurement of the actuator current is challenging due to the fast microdischarges occurring while the plasma is active. The morphology of the current signal is characterised by several high frequency, high amplitude peaks superimposed on a capacitive component of low frequency and amplitude. Several techniques have been applied (figure 24). A typical measurement method is the so-called shunt resistor technique [64, 68, 82, 157, 162]. This technique makes use of a resistor inserted in the path of the discharge current. To avoid problems with the high voltage the shunt resistor is typically inserted in series between the grounded electrode and the ground point. The resistor is subject to the discharge current (I) flowing through and based on Ohms law, a voltage (V_R) develops across:

$$V_R(t) = I(t)R \tag{4}$$

where R is the resistance. The voltage V_R can be sampled using a high speed oscilloscope.

An alternative method to measure current is via inductance [169]. When an inductor such as a coil is wrapped around a straight inductor such as the ground cable, the current developing in the former is proportional to the current of the latter. A typical current probe using this technique is the Rogowski coil which has been used extensively for both AC-DBD [63, 67, 95, 144, 146, 154] and ns-DBD [150, 163, 168]. In contrast to shunt resistor technique, Rogowski coils have limitations in frequency bandwidth. The high frequency limit is in the order of 500 MHz, while the low frequency limit is in the order of 100 Hz. This implies that using the Rogowski coil, resolution problems can arise for both the high frequency current spikes and the low frequency capacitive component [162].

A peer concept to the Rogowski coil is the Hall current sensor, albeit with a different working principle. The Hall effect develops when a magnetic field is applied perpendicularly to the flow of electrons through a conductor (the Hall

sensor). In that case Lorentz forces act on the flowing charge and deflect it from its straight line-of-sight trajectory. Due to the deflection a charge buildup is observed on one side of the conductor while a charge deficit is observed on the other side. The difference in charge is responsible for the development of a potential difference across the conductor, i.e. the Hall voltage. By applying a constant control current to the sensor, the Hall voltage becomes a sole function of the magnetic field. Commercial Hall current sensors are available with a ferrite loop which shields the sensor from stray magnetic fields. Typical bandwidths for Hall current sensors can be in the order 100 MHz. The loop can be placed around a conductor to be measured. This can be the ground cable to the plasma actuator [73, 113, 164, 165].

Shunt resistors, Rogowski coils and Hall sensors are straightforward and easy to apply techniques towards current measurements. Nevertheless, some uncertainties will occur in the estimation of the flowing current. The duration of microdischarges in a DBD is in the order of few nanoseconds and as such oscilloscopes capable of sampling rates of the order of GHz must be used. Additionally, the large amplitude of the current spikes in combination to the low amplitude displacement currents pose considerable requirements for the amplitude resolution of the oscilloscope. It is recommended to use resolutions of 16 bit or higher. More advanced techniques based on signal compression circuitry were described by Ashpis et al [162]. In this study the authors performed a careful comparison of current and power measurement techniques and concluded that even advanced high resolution oscilloscopes might be inadequate for time-resolved measurements of discharge currents in DBD plasma actuators. Despite these shortcomings, these are sufficient techniques for qualitative measurements of the discharge pattern, duration and intensity.

Electrical power is an important quantity for plasma actuators. Its accurate measurement is essential to parametric studies, characterisation and optimisation. Several techniques can be used depending on the type of actuator. For AC-DBD actuators the power can be calculated by simply multiplying the instantaneous values of measured current and applied voltage. The product can be integrated over a number of cycles in order to produce the time average power consumption. Although the technique has been used in some studies [64, 77, 112, 118, 159], the accuracy problems previously mentioned regarding

measurement of the discharge current are a limitation of this technique.

In order to bypass the resolution problems of direct current measurements, integral charge measurement techniques can be used [68, 86, 146, 161, 162] for power estimation. One such technique involves the use of a shunt capacitor inserted in series between the grounded electrode and the ground point in similar fashion to the shunt resistor technique. As the discharge current flows through the capacitor, charge is internally accumulated. The instantaneous accumulated charge (Q_M) in the capacitor is a function of the voltage across the leads (V_M) and the capacitance (C_M)

$$Q_M(t) = C_M V_M(t) \tag{5}$$

Furthermore, the current (I_c) throughout the capacitor, which is equal to the current through the actuator, is given by the rate of change of the accumulated charge

$$I_M(t) = \frac{\mathrm{d}Q_M}{\mathrm{d}t} = C_M \frac{\mathrm{d}V_M(t)}{\mathrm{d}t} \tag{6}$$

The instantaneous power can then be computed as the product of applied voltage (V) and current:

$$P(t) = V_a(t) C_M \frac{\mathrm{d}V_M(t)}{\mathrm{d}t} \tag{7}$$

The total power can then be integrated over a sufficiently large number of cycles [63, 101].

An extension of the shunt capacitor technique can be made by rearranging equation 7 and integrating over one cycle of actuation:

$$\begin{aligned} P_{av} &= \frac{1}{T} \int_0^T V(t) C \frac{\mathrm{d}V_c t}{\mathrm{d}t} \mathrm{d}t \\ &= \frac{1}{T} \int_0^T V_a(t) C_M \mathrm{d}V_M = \frac{1}{T} \int_0^T V_a(t) \mathrm{d}Q_M \end{aligned} \tag{8}$$

It is evident by equation 8 that the average power over one period (T) can be given by the integral of the applied voltage (V_a) as a function of accumulated capacitor charge (Q_M). This effectively means that the power can be calculated as the area enclosed by the V_a–Q_M curve in a Lissajous diagram (figure 25) divided by the period [82, 170].

The capacitor charge techniques present considerable advantages over direct current measurements. Due to the capacitor, the charge related to the individual microdischarges accumulates and is effectively integrated in time. This relaxes the requirements for extremely fast acquisition rates and increases the accuracy of measurement. Regarding the integral charge techniques, the shunt capacitor method requires the estimation of the time gradient of the voltage $\left(\frac{\mathrm{d}V_M(t)}{\mathrm{d}t} \right)$, which demands careful filtering and averaging of a sufficiently large number of cycles. In contrast the Lissajous curve technique does not require any differentiation, although careful filtering is also necessary in order to estimate the enclosed area accurately.
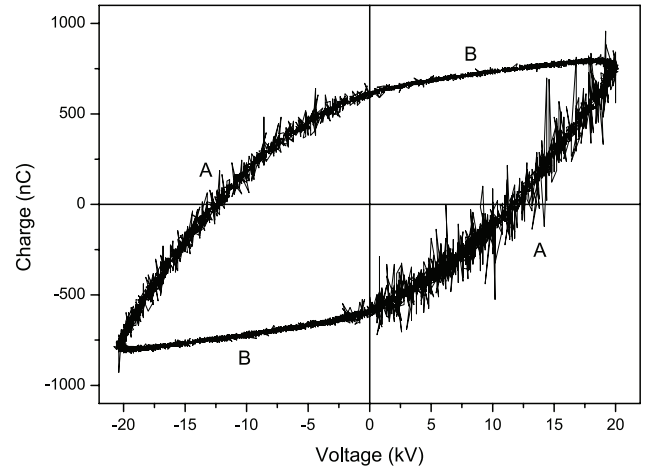

Figure 25. Typical Lissajous curve of voltage–charge for an AC-DBD actuator. Discharge is ignited in the quadrants denoted by *A* [68]. Reproduced with permission.

4.2. Voltage, current and power of ns-DBD actuators

Power measurements for ns-DBD present additional challenges compared to AC-DBD. Due to the timescales related to nanosecond pulses, the wave nature of the carried signal can no longer be neglected. In the case of AC-DBD actuators typical frequencies for the HV signal are in the order of kHz. Assuming a velocity factor (i.e. ratio of signal propagation speed to speed of light) of approximately 80% for standard cables, the wavelength of such signal can be as long as hundreds of meters. In contrast, for nanosecond pulses the relevant wavelength is in the order of micrometers. Consequently, the length of the transmission cable cannot be neglected. In this case, power losses due to radiation, reflections from cable discontinuities and impedance matching should be taken into consideration. As such, transmission line theory needs to be used for correct interpretation of voltage, current and power measurements regarding ns-DBD plasma actuators [171].

Notwithstanding the previous challenges, the measurement of voltage in the case of ns-DBD can be performed using fast high voltage probes [149, 151–153, 163]. The use of fast oscilloscopes with maximum sampling rate in the order of 1 GHz is essential. Additionally, care should be taken in using sufficiently long cabling in order to avoid superposition of the incoming and reflected HV pulse.

Current measurements can similarly be performed using shunt resistors [151, 153] or Rogowski coils [129, 150, 163, 166, 168, 172] inserted in series between the grounded electrode and ground point. It is important to note that reflections are evident also for the current pulses. As such, the incoming pulse is the current traveling through the actuator, while the reflected pulse is the current emitted back to the power supply (figure 26). The ground cable should be separated from the HV cable in order to avoid inductance currents.

A series of precautions is necessary for correctly interpreted power measurements for ns-DBD actuators. Firstly, it is more convenient to define pulse energy rather than power as the timescale separation between the pulse width ($O(ns)$) and pulse repetition ($O(ms)$) is large. As such, power can be assumed independent of
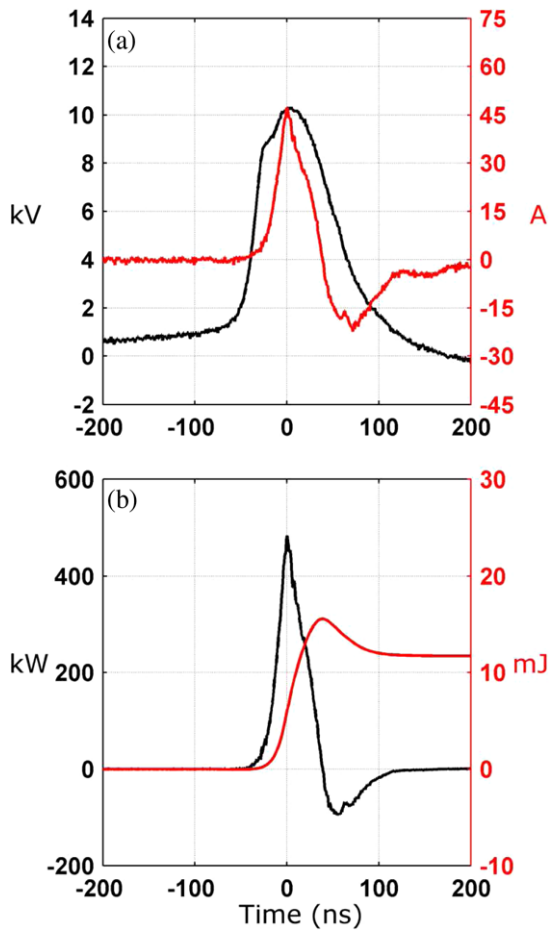
Figure 26. (a) Voltage and current and (b) power and energy of a ns-DBD actuator. Note the negative power due to the reflected pulse. Reproduced with permission from [151]. Copyright 2013, AIP Publishing LLC.

repetition frequency and only a function of individual pulse characteristics. Energy is then simply the product of high voltage and current integrated over the duration of the pulse [151]. Secondly, due to reflections, not all measured energy is used by the actuator. The energy corresponding to the product of the incoming voltage and current is what is provided by the power supply. The product of the reflected voltage and current is what is transferred back to the power supply. The net energy transferred by the actuator to the flow or diffused as losses is the difference between the incoming and reflected energies [40, 151, 153].

An alternative technique for measuring power associated with ns-DBD actuators is the so-called back-shunt current technique [40, 152]. This method requires no direct measurement of the HV signal and relies only on the measurement of the incident and reflected current through the actuator circuit. This is performed by simply inserting a resistor of sufficiently low nominal resistance in series to the ground shielding mesh of a coaxial HV cable. The cable needs to be sufficiently long (order of meters) and coaxial in order to ensure an inductance current pulse which is sufficiently separated between incidence and reflection. Additionally care should be taken to match the impedance of the HV cable to the impedance of the actuator in order to minimise unwanted reflections. Prior to the measurement the shunt needs to be calibrated. This is done

by sending a known low voltage signal through the actuator circuit and reading the output voltage across the shunt resistor. The ratio of the input and output voltage (K_{sh}) should be very close to the ratio of cable impedance and shunt resistance:

$$K_{sh} = \frac{Z}{R_{sh}} = \frac{V_a}{V_{sh}} \tag{9}$$

where Z is the impedance of the cable, R_{sh} is the shunt resistance, V_a is the applied voltage to the actuator and V_{sh} is the developed voltage across the shunt. Due to induction, the HV pulse travelling through the cable will create a flowing current through the ground mesh of the coaxial cable [171]. The current creates a voltage drop at the shunt resistor, which can be measured with a fast oscilloscope. The oscilloscope needs to match the impedance of the cable as close as possible. The energy of the pulse can then be calculated using:

$$E = \int_o^t V_a \cdot I \, dt = \int_0^t \frac{V_a^2}{Z} dt$$
$$= \int_0^t \frac{(V_{sh} \cdot K_{sh})^2}{Z} dt = \int_0^t \frac{(V_{sh} \cdot K_{sh})^2}{K_{sh} \cdot R_{sh}} \tag{10}$$

The net pulse energy will be the difference between the energy of the incident pulse and the energy of the reflected pulse.

4.3. Discharge characteristics

The discharge formation in DBDs in general and DBD actuators specifically can provide detailed insight into the underlying physical mechanisms governing the operation. A technique that has been frequently applied towards this goal is optical imaging of the discharge. This is usually performed using intensified charged-coupled device (iCCD) cameras [40, 63, 75, 82, 86, 153, 154, 160, 173]. These are digital cameras able to record light in the visible and invisible spectrum with a high signal-to-noise ratio. Typical for most iCCD is their ability to image fast processes with gate width times in the order of nanosecond [105, 157]. Through careful synchronisation with the applied voltage signal, iCCD imaging has revealed the highly asymmetric nature of the DBD discharge between the positive and negative half-cycles [82, 86] (figure 27) and the discharge structure due to positive or negative nanosecond pulses [163]. Debien et al [105] used this technique to demonstrate the effectiveness of thin wire electrode towards more uniform discharge patterns. Using extremely short gate times of 2 ns, Elias and Castera [129] were able to capture a ns-DBD actuator discharge propagating along the length of the electrodes (figure 28). An equivalent alternative to the use of iCCD cameras are photomultiplier tubes (PMT) [74, 118, 156].

Extending the optical imaging techniques, optical emission spectroscopy (OES) can provide a host of information regarding the active charged species in the plasma formation [144, 146]. The concept relies on the recording of the optical emission and the band pass filtering of selected wavelengths through prisms or diffraction gratings as described in section 3. The measured spectra can be fitted to numerical model predictions (usually using the SPECAIR commercial package) in order to extract information such as rotational,
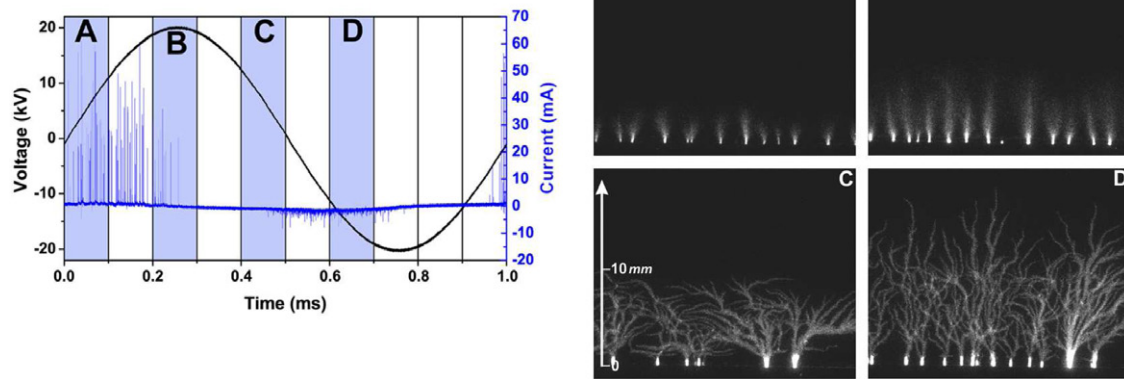
Figure 27. Discharge current and iCCD imaging of the plasma layer for a sine waveform. The imaging is done in the UV band for enhanced observability of the discharge. Note the strong asymmetry between plasma morphology during the positive and negative half-cycles. Reproduced with permission from [86]. Copyright 2012, AIP Publishing LLC.
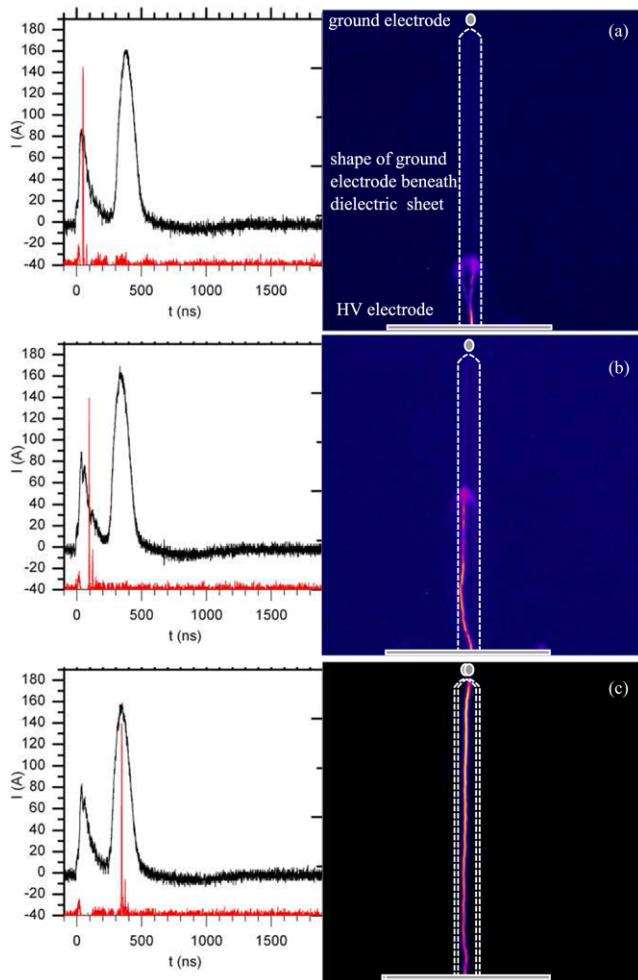

Figure 28. Synchronised discharge current and fast iCCD imaging of a ns-DBD configuration at different time delays. An extremely short shutter time of 2 ns allows the capture of the propagating discharge along the span of the actuator. The red peak signifies the timing of image acquisition [129]. Reproduced with permission.

vibrational and translational temperatures as well as reduced electric fields [40, 63, 145, 147].

Charge accumulation and potential distribution on the dielectric surface have been measured using an electrostatic voltmeter probe [73, 158, 164, 165]. This is a non-intrusive technique based on suspending the voltage probe over the dielectric surface without physical contact. An internal circuit is responsible for equalising the potential of the probe with the potential of the surface, thus providing an accurate measurement of the latter. The charge distribution can be further calculated simply by division with the elemental charge as shown by Cristofollini *et al* [164]. The electrostatic voltmeter probe has essentially no practical frequency response. As such the accumulated charge was estimated by performing the measurement after the actuator was switched off. The switching off was done at different phases of the applied high voltage while the electrostatic voltmeter probe was traversed along the plasma region. By reconstruction they were able to resolve the spatio-temporal evolution of the charge accumulation from 0 to 30 seconds after the end of the discharge.

Opaits *et al* [158] used this technique and showed that charge accumulation is a significant factor contributing to reduced ability of the actuator to force the flow. They proposed the use of a DC HV signal with repetitive nanosecond pulses instead of the typical sinusoidal AC signal. They demonstrated an improvement in actuator performance using such powering configuration. Font *et al* [128] used the V-dots approach, where they segmented the covered electrode in individual isolated pieces (figure 29). They then measured the displacement current through each segment using an integrating circuit composed from a resistor and a capacitor. In order to further separate between surface charge and charges on the exposed electrode they calibrated their measurement using applied voltages low enough to prohibit plasma formation, thus attaining a functional relationship between purely electrode charge and applied voltage. Similar approach was followed by Nichols and Rovey [167] where they acquired charge accumulation as well as electric field values on the surface.

5. Effect of ambient conditions

Although the performance of DBD actuators is well documented in laboratory conditions, they are intended for operation in a variety of non-standard environments. Aerospace
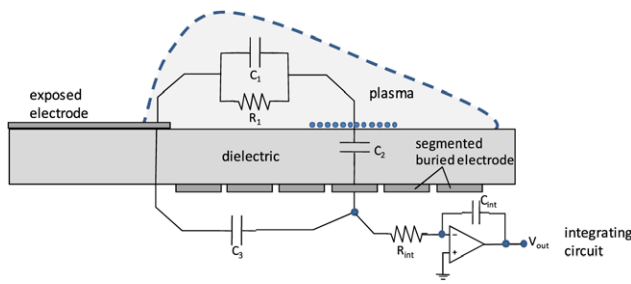
Figure 29. Segmented ground electrode arrangement along with an integrating circuit used by Font *et al* in order to measure surface charging on an AC-DBD actuator [128]. Reproduced with permission.

applications will demand operation in high altitude where low temperatures, low ambient pressures and low humidity levels are encountered in comparison to sea level. In contrast, wind turbine applications will expose the actuators to environment of increased humidity, debris and acidic conditions such as salt water. Finally, applications in high speed aerodynamics and turbomachinery will necessitate operation under elevated ambient and surface temperatures and even with other than air gases [174]. Several recent studies approached the effect of external, ambient conditions on aspects of plasma actuator performance. Although, not directly affecting the chosen diagnostic techniques, ambient conditions are treated in this review due to their important role in the characterisation of plasma actuators. An overview on investigations on the effect of ambient conditions is given in table 5.

5.1. Effect of ambient pressure and working gas composition

Ambient pressure has a profound effect on the performance of plasma actuators. Studies have been conducted by operating the actuator in vacuum chambers where the ambient pressure can be regulated in a range of lower and higher than atmospheric pressures. Several diagnostics have been used including induced velocity, integrated force, current, power and optical emissions.

The induced velocity and produced force follow non-linear, non-monotonic behaviour with varying pressure [125, 126, 177, 184]. Abe *et al* [126] investigated the effect of pressures from 1 to 0.25 atm in a vacuum chamber (figure 30), using force and velocity measurements. The velocity and force increased while decreasing pressure from 1 to 0.6 atm. With further decreasing pressure, force and velocity decrease. Similar results were shown by Benard *et al* [177] using more elaborate velocity measurements. Versailles *et al* [125] used PIV for ambient pressure values higher than atmospheric (1–2.7 atm). They confirmed that the previously observed trends are valid for this range as well, i.e. the actuator induced velocity magnitude degrades non-linearly with increasing pressure above 1 atm.

Power is severely affected by ambient pressure. A monotonic behaviour has been registered in several studies with the consumed power increasing quadratically with decreasing pressure [126, 177]. This can be attributed to changes in high frequency current spikes during the positive half cycle [179]. The power increase trend is followed closely by the

plasma extent length as shown by optical imaging [167, 177, 182], suggesting an increase in the mean free path of particles. As the pressure decreases the discharge transitions from filamentary to diffuse [188]. Additionally, Nichols and Rovey [167] measured surface charge and electric field for decreasing pressure. They showed that although plasma extent is increased with decreasing pressure, this is happening in an area where the electric field is very small and as such the produced force is weak. This confirms the low forces and velocities measured by Abe *et al* [126] for low pressures. Finally, ambient pressure appears to affect the limits of electrical breakdown of the working gas. The minimum breakdown voltage decreases almost linearly with pressure for a range of 0.2–1 atm. For a larger range of pressures (0.2–9 atm) a piecewise linear increase of breakdown voltage has been observed [184].

The composition of the working gas is not likely to be a variable in plasma actuator applications as aerodynamic flow control devices. Yet the study of their performance in these conditions can provide useful insight into their working principles. In general produced force and induced velocity is lower for pure nitrogen than for air [75, 126, 138]. The addition of oxygen to the working fluid increases produced force during the forward stroke and overall efficiency of the actuator, where efficiency can be defined as thrust over power [92, 128, 138]. The time resolved measurements of Font *et al* [128] and Leonov *et al* [75] clearly show the important role negative ions and the forward stroke (negative half-cycle) have in the momentum production process.

### 5.2. Effect of temperature and humidity

Air temperature variations can be encountered not only in altitude operation but also in internal flows typically found in turbomachinery. Force and power measurements of AC-DBD actuators have been conducted by Versailles *et al* [125] for a range of ambient temperatures spanning from 30 to 200 °C. They report an almost linear increase of produced force with temperature. Power consumption is also increased. They attribute the increase in both force and power to a possible decrease of the mean free path for collisional particles due to decrease of the gas density.

Erfani *et al* [180] studied the effect of dielectric temperature on the performance of an AC-DBD actuators. They enforced lower (−40 °C) and higher (120 °C) than room temperatures using dry ice and a Peltier heater respectively. PIV measurements of the induced velocity confirmed the observed trends of Versailles *et al* [125]. On a similar study, Durscher *et al* [117] demonstrated that the dielectric surface temperature can affect the thrust saturation effect common in AC-DBD actuators. They showed that increasing surface temperature would delay the saturation effect, thus allowing the actuator to operate at higher carrier frequencies without the loss of efficiency. Aba'a Ndong *et al* [185] studied the effect of dielectric ageing under ns-DBD actuation. They showed an increase of discharge non-uniformities when using an aged actuator along with an increase of dissipated power.

Humidity has been shown to affect the electrical and mechanical behaviour of the actuator dramatically [178].

Table 5. Overview of investigations on effect of ambient conditions.

Reference	Conditions	Voltage (p–p) [kV]	Frequency [kHz]	Actuator type
Labergue *et al* (2004) [175]	external flow	30	DC	DC corona
Enloe *et al* (2006) [138]	gas	16	5	AC-DBD
Pavon *et al* (2007) [176]	external airflow	14	1–15	AC-DBD
Abe *et al* (2008) [126]	ambient pressure, gas	12–20	1–5	AC-DBD
Benard *et al* (2008) [177]	ambient pressure	32	1	AC-DBD
Benard *et al* (2009) [178]	relative humidity	32–48	1	AC-DBD
Leonov *et al* (2010) [75]	gas	24	0.02–2	AC-DBD
Versailles *et al* (2010) [125]	ambient pressure, temperature	15–20.5	10–17	AC-DBD
Ashpis and Thurman (2011) [174]	air density	generic		AC-DBD
Hollick *et al* (2011) [179]	ambient pressure	12.7	13	AC-DBD
Font *et al* (2011) [128]	gas	14–30	0.2	AC-DBD
Durscher *et al* (2012) [117]	dielectric temperature	20–46	2–7	AC-DBD
Erfani *et al* (2012) [180]	dielectric temperature	2–8	10	AC-DBD
Erfani *et al* (2012b) [181]	external flow	15	10	AC-DBD
Khramtsov *et al* (2012) [182]	ambient pressure			AC-DBD
Kriegseis *et al* (2012) [183]	external flow	16–26	8–14	AC-DBD
Valerioti and Corke (2012) [184]	ambient pressure	11.5–21	1–5	AC-DBD
Aba'a Dong *et al* (2013) [185]	dielectric ageing	10	single pulse	ns-DBD
Nichols and Rovey (2013) [167]	ambient pressure	13.4	5	AC-DBD
Pereira *et al* (2013,2014) [123, 186]	external flow	40	2	AC-DBD
Kriegseis *et al* (2013) [187]	external flow	10–28	8–11	AC-DBD
Wu *et al* (2013) [188]	ambient pressure	10	23	AC-DBD
Kriegseis *et al* (2014) [189]	ambient pressure, external flow	17	9	AC-DBD
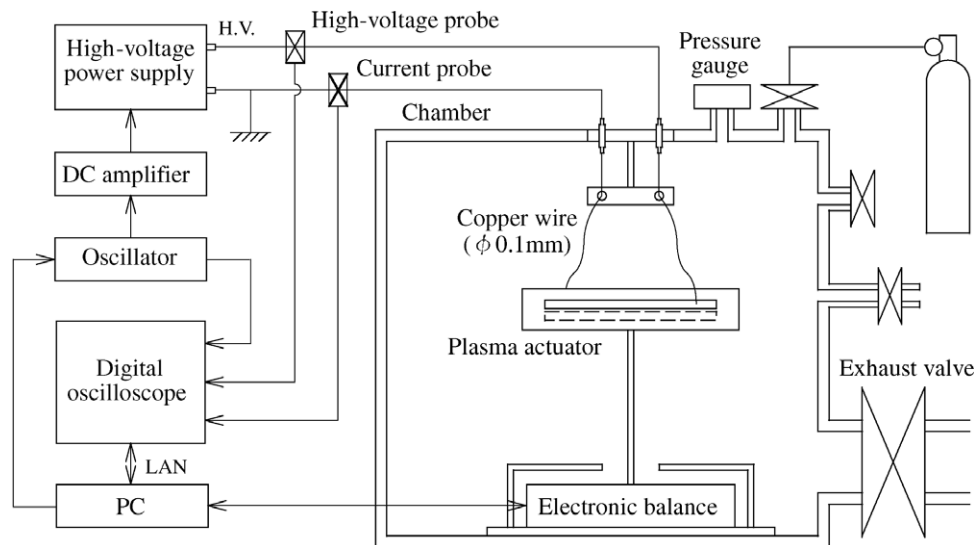
Figure 30. The vacuum chamber used by Abe *et al* in an investigation of the effect of ambient pressure and gas composition on the performance of an AC-DBD actuator. From [126]; reprinted by permission of the American Institute of Aeronautics, Inc.

An AC-DBD actuator has been tested in an enclosed vessel containing an ultrasonic water atomiser. LDV velocity measurements and shunt resistor current measurements were conducted for a relative humidity range spanning from 40% to 98%. It was shown that the electrical power consumption of the actuator decreases with increasing humidity of up to 85%. For relative humidity over 85% the power sharply increases due to condensation on the dielectric surface. Similar behaviour of decreasing power has been reported for DC-corona actuators [5] for the range of 41% to 49% relative humidity. The induced velocity decreases with increasing humidity although the actuator appears to be able to transfer momentum even at high humidity levels. In contrast to previous work, recent investigations by Wilkinson *et al* [190] showed contradicting trends for thrust as a function of humidity. Different dielectric material demonstrated completely reversed behaviour i.e. thrust increase with increasing humidity. The tests were performed in a controlled humidity environment using a humidifier. This raises the question whether it is better for humidity to be controlled or just measured for this kind of investigations.

5.3. Effect of external velocity

One of the most important aspects of the effect of external conditions on the performance of plasma actuators is the influence of external velocity. Early modelling and experimental studies have unequivocally argued that the timescales involved in the plasma production and sustainment processes are sufficiently separated from the hydrodynamic time scales encountered during flow control [2, 60]. Based on this assumption many investigations assume that the external flow does not affect the performance of the actuator and, as such, modelling or diagnostics in quiescent conditions is sufficient for mapping the actuator.

Several studies have instead shown a strong dependency of the actuator performance on the existence and strength of external flow [123, 175, 176, 181, 183, 186, 189]. In an early study Labergue *et al* [175] measured electrical current on a DC-corona actuator positioned on the sharp trailing edge of a flat plate under external velocity of 0 to 35 ms^{-1}. They showed a pronounced increase in discharge current for increasing free stream velocity. Additionally they observed a stabilisation effect on the glow discharge associated with an increase in the space charge density.

The effect of external flow has also been evident on the performance of AC-DBD actuators. The breakdown voltage has been found to increase with increasing velocity [176]. This has been attributed to the purging of highly energetic metastables of nitrogen out of the discharge region during one HV cycle. This necessitates higher voltages in order to sustain discharge. An important effect is also the change from the glow to the filamentary regime due to increase of external velocity [176]. Additionally, the number of microdischarges reduces as the external flow carries energetic species out of the strong electric field region [181].

Electrical power is increased considerably under external flow [183, 187]. This is accompanied by a profound luminosity decrease suggesting the previously observed mechanisms of metastables depletion [176]. In general, increasing airflow velocity and decreasing pressure seem to have a similar effect, both increasing power. In contrast, they compete regarding luminosity where the former increases with decreasing pressure but decreases with increasing velocity [189].

In spite of several studies indicating the influence of airflows on the actuators power, current and optical emissions, a very limited number of studies focus on the plasma-neutral momentum transfer. As mentioned earlier, the general model assumes no functional relationship between plasma forcing and external flow due to time scale separation. In a recent study Pereira *et al* [123, 186] measured the reaction force of an AC-DBD actuator under quiescent and external flow conditions for both co-flow and counter-flow configurations. Although they observed little dependence of the measured force on the external flow their results are inconclusive regarding the momentum transfer ability of the actuator for external velocities larger than 60 ms^{-1}. Under these conditions the fluid transport velocity starts to approach the drift velocity of the heavy species (ions and negative ions). Pereira *et al* [123] proposed a simple phenomenological model to account for

this. They show that the force transferred by the plasma to the neutral fluid can be decreased up to 30% for free stream velocity of 200 ms^{-1} compared to quiescent conditions.

6. Open issues and future directions

Experimental characterisation techniques, whether mechanical, thermal or electrical, are essential towards elucidating the complex physical principles behind the operation of plasma actuators. For every answer these studies provide, they create additional questions. Yet, the ever increasing number of research groups that work on this topic is both reassuring for the potential of these actuators and promising for bringing them closer to industrial applications. Many aspects of plasma actuator characterisation studies can be challenging due to extremely weak effects to be measured (small velocities and forces), the requirements for measuring under environments of high voltage and the multitude of spatio-temporal scales involved. Nevertheless, the attention, labour and technical solutions given by the workers in the field towards overcoming these challenges is impressive. In this last section some open issues and directions for further improvement of plasma actuator diagnostics are given. It must be stressed that this list is far from complete and can only serve as a starting point for the venturing experimentalist in this exciting field.

6.1. Tracer particles in strong electric fields

Optical velocimetry techniques such as PIV and LDV have been proven to be extremely powerful tools towards the in-depth characterisation of the mechanical behaviour of the actuator. Capitalising on the high spatio-temporal resolution of LDV, workers have been able to resolve the in-cycle fluctuation of the induced velocity [80, 85]. Similarly, PIV has been used for phase-locked measurements of the full spatio-temporal resolution of the velocity field [100, 135]. Additionally, PIV- and LDV-measured velocity fields have been used in order to derive the plasma induced body force using a variety of techniques [87, 97, 104, 132].

PIV and LDV techniques necessitate the use of tracer particles, which need to meet a series of requirements in order to produce an accurate velocity measurement [107]. Firstly they need to be able to follow the movement of the gas without interfering or lagging. The highest velocity fluctuation that the particles can faithfully follow is generally a function of their size. Tracer particles in the order of 1 μm in size have a low-pass frequency higher than 100 kHz [191, 192] which is well above typical actuator frequencies. Unfortunately, the nature of the operation of plasma actuators imposes further constraints on tracer particles. The extremely strong electrical field in the plasma region imposes the risk of charging, magnetising or even chemical breakdown of the tracer particles. In this case, the movement of the tracers is no longer the movement of the gas but the one dictated by the electrical field. Naturally, whether the tracer particles become charged is a function of their size and material [102]. Few studies have dealt with this issue and only as a secondary effect [102, 103, 108–110]. A

larger amount of careful calibration studies comparing seeded and non-seeded flows with independent measurement techniques are of paramount importance for the establishment of optical velocimetry techniques as a mainstay of plasma characterisation tools. The challenge in this endeavour lies in identifying the fidelity of PIV or LDV measurements not only in resolving the time-average induced velocities but also the time- or phase-resolved behaviour. The main problem is devising a technique that can act as a reference case for non-seeded flows. To the author's knowledge no conventional opto-mechanical measurement technique exists through which the time resolved flow field in the vicinity of the plasma region can be measured in an unobtrusive manner without the use of tracer particles. It appears that a candidate might be molecular tagging velocimetry [193], although the issues with the application of such a technique for plasma actuators are quite unknown.

6.2. Spatio-temporal body force distribution

The experimental determination of the spatio-temporal body force distribution has been a holy grail for some groups. This is not only due to the challenging nature of this endeavour but also due to its profound merits towards understanding, modelling and tailoring the actuators for flow control. The general idea is based on derivation of the body force field from velocity data. Several techniques have been proposed using some form of the constitutive equations of fluid motion, namely the Navier–Stokes equations. The velocity data come usually from PIV or LDV measurements.

The unsteady acceleration, convective and diffusive terms of the NS (equation 3) are readily available while body force and pressure gradient terms are unknown. Wilke [132] and other workers from the group of Darmstadt University [87, 88] suggest that the pressure gradient term is relatively small compared to the body force and thus can be neglected. They base this on good agreement between numerical simulation of the quiescent flow using their experimentally derived body force and the measured velocity field. Additionally, their simulation produces a very small pressure gradient indeed. Care needs to be taken regarding the assumption of a negligible pressure gradient. In commercial incompressible CFD the pressure term has no independent equation and as such needs to be calculated iteratively using the computed velocity (for example using the SIMPLE algorithm). In Wilke's simulations the source term contains both body force and pressure gradient. Irrespective of the magnitude of the pressure gradient, the simulation will produce the correct flow field without the need for producing any pressure gradient since this is already included in the body force term. As such one can never be certain if the pressure gradient term can be neglected or not. In reality, experimental evidence [97, 138] and numerical simulations [194] suggest that pressure gradient is far from negligible.

Albrecht *et al* [136] followed a different approach where they use the velocity vorticity formulation in order to eliminate the pressure gradient term. They further assume that the horizontal gradient of vertical force is negligible in order to integrate the horizontal component. Especially the first assumption needs to be scrutinised. The body force can be

assumed to be an arbitrary vector field. According to the Helmholtz theorem such a field can be decomposed into the sum of a curl-free and divergence-free field. By using the velocity-vorticity formulation the curl-free part of the body force is lost. It is not clear how dominant this component is compared to the total body force field.

The method proposed by Kotsonis *et al* [97] is based on the main assumption of a quasi-steady body force. As such, the technique cannot take into account the temporal variation of the force within the high voltage cycle. Additionally, for low carrier frequency the method will fail altogether as the characteristic time of the accelerating flow field (several milliseconds) approaches the forcing period.

It is, therefore, evident from published research that rigorous derivation of the plasma body force using experimental velocity fields is very challenging. If the full spatio-temporal distribution is sought and the pressure gradient is not neglected, then the system becomes underdetermined. Especially the separation of the pressure gradient and the curl-free component of the body force is impossible by just using the NS equations. Further development of these techniques is certainly needed. A possible route might be the closure of the system by using some of Maxwell's equations with additional diagnostics such as charge distribution. Alternatively, a combined use of experiments and CFD could be used in a conjugate manner in order to derive a body force that can replicate (in CFD) the experimentally observed flow fields. Great attention should be put in what exactly the CFD solver is solving for in order to avoid ambiguities between pressure gradient and body force.

6.3. ns-DBD actuators

Nanosecond-pulsed DBD actuators have received considerably less attention than AC-DBD actuators in characterisation studies. Conversely, it seems that their flow control authority on the specific case of leading edge stall control is equal or even greater. The flow control mechanism attributed to ns-DBD actuators is identified as a primarily thermal effect. The majority of studies have focussed on the *footprint* of the rapid energy deposition which is manifested as weak compression waves [40, 150, 151]. On the other hand it seems unlikely that these waves are the actual flow control mechanism. Long after the shock waves leave the area of the actuator an area of intense gas heating remains which can be responsible for strong density and/or viscosity gradients [152]. Careful characterisation of such effects is essential for the elucidation of the flow control principle of ns-DBDs. Similar to AC-DBD, field velocity diagnostics, such as PIV, can be of great use in this area. In theory, the density/viscosity perturbations due to ns-DBD can be extracted form time- or phase-resolved velocity measurements using decompositions of the compressible Navier–Stokes equations. In fact current efforts from the author's group towards this goal are under way.

6.4. Effect of ambient conditions

Although the majority of characterisation studies is conducted in quiescent conditions, these are devices which are

meant for operation in a wide variety of environments. Several studies have been published regarding the effect of ambient temperature, pressure, gas composition and humidity on the electromechanical performance of the actuators. The effects of pressure and temperature are of particular importance for aerospace applications.

Additionally the effect of external flow has received some attention as results clearly show a two-way coupling between the flow and the discharge. This has far-reaching implications to the long standing norm regarding the AC-plasma actuator body force. The commonly accepted practice in both actuator modelling and implementation in CFD studies is that the body force is independent of the external velocity. This is based on the large separation of time-scales governing the discharge on one hand and the flow on the other. Yet, for higher free stream velocities, the collisional model of momentum transfer can no longer be valid since the transport velocity of neutral particles is approaching the drift velocity of the heavy charged species [123]. It is essential, for securing the application potential of these actuators, that accurate force and momentum transfer measurements are conducted in conditions of external flow.

Acknowledgments

References

[1] Aristotle *Metaphysics*
[2] Corke T C, Enloe C L and Wilkinson S P 2010 Dielectric barrier discharge plasma actuators for flow control *Annu. Rev. Fluid Mech.* **42** 505–29
[3] Benard N and Moreau E 2014 Electrical and mechanical characteristics of surface ac dielectric barrier discharge plasma actuators applied to airflow control *Exp. Fluids* **55** 1–43
[4] Roth J, Sherman D and Wilkinson S 1998 *Boundary Layer Flow Control with a One Atmosphere Uniform Glow Discharge Surface Plasma* (Reston, VA: American Institute of Aeronautics and Astronautics)
[5] Leger L, Moreau E and Touchard G 2001 Control of low velocity airflow along a flat plate with a dc electrical discharge *Industry Applications Conf., 2001. Thirty-Sixth IAS Annual Meeting. Conf. Record of the 2001 IEEE* vol 3 pp 1536–43
[6] Roupassov D V, Nikipelov A A, Nudnova M M and Starikovskii A Y 2008 Flow separation control by plasma actuator with nanosecond pulse periodic discharge *46th AIAA Aerospace Sciences Meeting and Exhibit*
[7] Samimy M, Adamovich I, Webb B, Kastner J, Hileman J, Keshav S and Palm P 2004 Development and characterization of plasma actuators for high-speed jet control *Exp. Fluids* **37** 577–88
[8] Schutze A, Jeong J Y, Babayan S E, Park J, Selwyn G S and Hicks R F 1998 The atmospheric-pressure plasma jet: a review and comparison to other plasma sources *IEEE Trans. Plasma Sci.* **26** 1685–94

[9] Fridman A, Chirokov A and Gutsol A 2005 Non-thermal atmospheric pressure discharges *J. Phys. D: Appl. Phys.* **38** R1–R24
[10] Loeb L B 1965 *Electrical Coronas: Their Basic Physical Mechanism* (Berkeley, CA: University of California Press)
[11] Goldman M and Goldman N 1978 *Gaseous Electronics* (New York: Academic Press)
[12] Robinson M 1961 Movement of air in the electric wind of the corona discharge *AIEE Trans.* **80** 143–50
[13] Robinson M 1962 A history of the electric wind *Am. J. Phys.* **30** 366–72
[14] von Guericke O 1672 *Experimenta Nova Magdeburgica* (Amsterdam: De Vacuo Spatio) pp 147–50
[15] Hauksbee F 1709 *Physico-Mechanical Experiments on Various Subjects* printed by R Brugis for the author (London) pp 46–7
[16] Faraday M 1839 *Experimental Researches in Electricity* **1** (London: Quaritch)
[17] Velkoff H and Ketchman J 1968 Effect of an electrostatic field on boundary layer transition *AIAA J.* **6** 1381–3
[18] Velkoff H R and Godfrey R 1979 Low-velocity heat transfer to a flat plate in the presence of a corona discharge in air *Trans. ASME, J. Heat Transfer* **101** 157–63
[19] Malik M R, Weinstein L and Hussaini M 1983 Ion wind drag reduction *AIAA Meeting*
[20] Noger C, Touchard G and Chang J S 1997 Active control of cylinder in cross flow by corona discharge induced ehd secondary flow *Proc. 2nd Int. Symp. Plasma Techn. Polution Cont, Bahia* pp 136–41
[21] Artana G, D'Adamo J, Leger L, Moreau E and Touchard G 2002 Flow control with electrohydrodynamic actuators *AIAA J.* **40** 1773–9
[22] Siemens W 1857 Ueber die elektrostatische Induction und die Verzögerung des Stroms in Flaschendräten *Ann. Phys. Chem.* **102** 66–120
[23] Langmuir I 1928 Oscillations in ionized gases *Proc. Natl Acad. Sci. USA* **14** 627–37
[24] Kunhardt E E 2000 Generation of large-volume, atmospheric-pressure, nonequilibrium plasmas *IEEE Trans. Plasma Sci.* **28** 189–200
[25] Buss K 1932 Die elektrodenlose Entladung nach Messung mit dem Kathodenoszillographen *Arch. Elektrotech.* **26** 261–5
[26] Klemenc A, Hinterberger H and Hofer H 1937 *Z. Elektrochem.* **43** 708
[27] Kanazawa S, Kogoma M, Moriwaki T and Okazaki S 1988 Stable glow plasma at atmospheric pressure *J. Phys. D: Appl. Phys.* **21** 838–40
[28] Kanazawa S, Kogoma M, Okazaki S and Moriwaki T 1989 Glow plasma treatment at atmospheric pressure for surface modification and film deposition *Nucl. Instrum. Methods Phys. Res.* B **37–8** 842–5
[29] Yokoyama T, Kogoma M, Kanazawa S, Moriwaki T and Okazaki S 1990 Improvement of the atmospheric-pressure glow plasma method and the deposition of organic films *J. Phys. D: Appl. Phys.* **23** 374–7
[30] Okazaki S, Kogoma M, Uehara M and Kimura Y 1993 Appearance of stable glow discharge in air, argon, oxygen and nitrogen at atmospheric pressure using a 50 Hz source *J. Phys. D: Appl. Phys.* **26** 889–92
[31] Kogelschatz U, Eliasson B and Egli W 1997 Dielectric-barrier discharges principle and applications *J. Physique* **7** 47–66
[32] Kogelschatz U 2003 Dielectric-barrier discharges: their history, discharge physics, and industrial applications *Plasma Chem. Plasma Process.* **23** 1–46
[33] Reece Roth J, Sherman D M and Wilkinson S P 2000 Electrohydrodynamic flow control with a glow-discharge surface plasma *AIAA J.* **38** 1166–72
[34] Vasilyak L M, Kostyuchenko S V, Kudryavtsev N N and Filyugin I V 1994 High-speed ionization waves at an electric breakdown *Usp. Fiz. Nauk* **164** 263–86

[35] Starikovskaia S M 1995 *Plasma Phys. Rep.* **21** 541–7

[36] Starikovskaia S M, Starikovskii A Y and Zatsepin D V 1998 The development of a spatially uniform fast ionization wave in a large discharge volume *J. Phys. D: Appl. Phys.* **31** 1118–25

[37] Starikovskii A Y 2005 Plasma supported combustion *Proc. Combust. Inst.* **30** 2405–17

[38] Starikovskaia S M 2014 Plasma-assisted ignition and combustion: nanosecond discharges and development of kinetic mechanisms *J. Phys. D: Appl. Phys.* **47** 353001

[39] Roupassov D V, Nikipelov A A, Nudnova M M and Starikovskii A Y 2008 Boundary layer separation control by nanosecond plasma actuator *44th AIAA/ASME/SAE/ASEE Joint Propulsion Conf. and Exhibit*

[40] Starikovskii A Y, Nikipelov A A, Nudnova M M and Roupassov D V 2009 Sdbd plasma actuator with nanosecond pulse-periodic discharge *Plasma Sources Sci. Technol.* **18** 034015

[41] Post M L and Corke T C 2004 Separation control on high angle of attack airfoil using plasma actuators *AIAA J.* **42** 2177–84

[42] Huang J, Corke T C and Thomas F O 2006 Plasma actuators for separation control of low-pressure turbine blades *AIAA J.* **44** 51–7

[43] Labergue A, Moreau E, Zouzou N and Touchard G 2007 Separation control using plasma actuators: application to a free turbulent jet *J. Phys. D: Appl. Phys.* **40** 674–84

[44] Little J and Samimy M 2010 High-lift airfoil separation with dielectric barrier discharge plasma actuation *AIAA J.* **48** 2884–98

[45] Little J, Takashima K, Nishihara M, Adamovich I and Samimy M 2012 Separation control with nanosecond-pulse-driven dielectric barrier discharge plasma actuators *AIAA J.* **50** 350–65

[46] Hultgren L S and Ashpis D E 2003 Demonstration of separation delay with glow-discharge plasma actuators *41st Aerospace Sciences Meeting and Exhibit*

[47] Grundmann S and Tropea C 2008 Active cancellation of artificially introduced Tollmien-Schlichting waves using plasma actuators *Exp. Fluids* **44** 795–806

[48] He C, Corke T C and Patel M P 2009 Plasma flaps and slats: an application of weakly ionized plasma actuators *J. Aircr.* **46** 864–73

[49] Kotsonis M, Pul R and Veldhuis L 2014 Influence of circulation on a rounded-trailing-edge airfoil using plasma actuators *Exp. Fluids* **55** 1–4

[50] Thomas F O, Kozlov A and Corke T C 2008 Plasma actuators for cylinder flow control and noise reduction *AIAA J.* **46** 1921–31

[51] Nati G, Kotsonis M, Ghaemi S and Scarano F 2013 Control of vortex shedding from a blunt trailing edge using plasma actuators *Exp. Therm. Fluid Sci.* **46** 199–210

[52] Nishihara M, Takashima K, Rich J W and Adamovich I V 2011 Mach 5 bow shock control by a nanosecond pulse surface dielectric barrier discharge *Phys. Fluids* **23** 066101

[53] Lombardi A J, Bowles P O and Corke T C 2013 Closed-loop dynamic stall control using a plasma actuator *AIAA J.* **51** 1130–41

[54] Suzen Y B, Huang P G, Jacob J D and Ashpis D E 2005 Numerical simulations of plasma based flow control applications *35th AIAA Fluid Dynamics Conf. and Exhibit*

[55] Orlov D M and Corke T C 2005 Numerical simulation of aerodynamic plasma actuator effects *43rd AIAA Aerospace Sciences Meeting and Exhibit: Meeting Papers* pp 10045–56

[56] Singh K P and Roy S 2005 Simulation of an asymmetric single dielectric barrier plasma actuator *J. Appl. Phys.* **98** 083303

[57] Boeuf J P, Lagmich Y, Unfer Th, Callegari Th and Pitchford L C 2007 Electrohydrodynamic force in dielectric barrier discharge plasma actuators *J. Phys. D: Appl. Phys.* **40** 652–62

[58] Unfer T and Boeuf J P 2009 Modelling of a nanosecond surface discharge actuator *J. Phys. D: Appl. Phys.* **42** 194017

[59] Corke T C, Post M L and Orlov D M 2007 Sdbd plasma enhanced aerodynamics: concepts, optimization and applications *Prog. Aerosp. Sci.* **43** 193–217

[60] Moreau E 2007 Airflow control by non-thermal plasma actuators *J. Phys. D: Appl. Phys.* **40** 605–36

[61] Corke T C, Post M L and Orlov D M 2009 Single dielectric barrier discharge plasma enhanced aerodynamics: physics, modeling and applications *Exp. Fluids* **46** 1–26

[62] Liu B, Wang L, Luo Z B, Xia Z and Deng X 2012 Review of actuators for high speed active flow control *Sci. China* **55** 2225–40

[63] Dong B, Bauchire J M, Pouvesle J M, Magnier P and Hong D 2008 Experimental study of a DBD surface discharge for the active control of subsonic airflow *J. Phys. D: Appl. Phys.* **41** 155201

[64] Forte M, Jolibois J, Pons J, Moreau E, Touchard G and Cazalens M 2007 Optimization of a dielectric barrier discharge actuator by stationary and non-stationary measurements of the induced flow velocity: application to airflow control *Exp. Fluids* **43** 917–28

[65] Chue S H 1975 Pressure probes for fluid measurement *Prog. Aerosp. Sci.* **16** 147–223

[66] Moreau E, Louste C and Touchard G 2008 Electric wind induced by sliding discharge in air at atmospheric pressure *J. Electrost.* **66** 107–14

[67] Thomas F O, Corke T C, Iqbal M, Kozlov A and Schatzman D 2009 Optimization of dielectric barrier discharge plasma actuators for active aerodynamic flow control *AIAA J.* **47** 2169–78

[68] Pons J, Moreau E and Touchard G 2005 Asymmetric surface dielectric barrier discharge in air at atmospheric pressure: electrical properties and induced airflow characteristics *J. Phys. D: Appl. Phys.* **38** 3635–42

[69] Porter C, Abbas A, Cohen K, McLaughlin T and Enloe C L 2009 Spatially distributed forcing and jet vectoring with a plasma actuator *AIAA J.* **47** 1368–78

[70] Jacob J D, Ramakumar K, Anthony R and Rivir R B 2005 Control of laminar and turbulent shear flows using plasma actuators *4th Int. Symp. on Turbulence and Shear Flow Phenomena* vol 2 pp 653–8

[71] Kotsonis M and Ghaemi S 2012 Experimental and numerical characterization of a plasma actuator in continuous and pulsed actuation *Sensors and Actuators* **187** 84–94

[72] Moreau E, Leger L and Touchard G 2006 Effect of a dc surface-corona discharge on a flat plate boundary layer for air flow velocity up to 25 ms^{-1} *J. Electrost.* **64** 215–25

[73] Neretti G, Cristofolini A and Borghi C A 2014 Experimental investigation on a vectorized aerodynamic dielectric barrier discharge plasma actuator array *J. Appl. Phys.* **115** 163304

[74] Magnier P, Hong D, Leroy-Chesneau A, Pouvesle P and Hureau J 2007 A dc corona discharge on a flat plate to induce air movement *J. Electrost.* **65** 655–9

[75] Leonov S, Opaits D, Miles R and Soloviev V 2010 Time-resolved measurements of plasma-induced momentum in air and nitrogen under dielectric barrier discharge actuation *Phys. Plasmas* **17** 113505

[76] Jukes T N, Choi K, Johnson G A and Scott S J 2006 Characterization of surface plasma-induced wall flows through velocity and temperature measurements *AIAA J.* **44** 764–71

[77] Kotsonis M and Veldhuis L 2010 Experimental study on dielectric barrier discharge actuators operating in pulse mode *J. Appl. Phys.* **108** 113304

[78] Lomas C G 1986 *Fundamentals of Hot Wire Anemometry* (Cambridge: Cambridge University Press)

[79] Jukes T N, Choi K, Segawa T and Yoshida H 2008 Jet flow induced by a surface plasma actuator *Proc. Inst. Mech. Eng.* **222** 347–56

[80] Forte M, Leger L, Pons J, Moreau E and Touchard G 2005 Plasma actuators for airflow control: measurement of the non-stationary induced flow velocity *J. Electrost.* **63** 929–36

[81] Porter C O, Baughn J W, McLaughlin T E, Enloe C L and Font G I 2007 Plasma actuator force measurements *AIAA J.* **45** 1562–70

[82] Joussot R, Leroy A, Weber R, Rabat H, Loyer S and Hong D 2013 Plasma morphology and induced airflow characterization of a dbd actuator with serrated electrode *J. Phys. D: Appl. Phys.* **46** 125204

[83] Drain L E 1980 *The Laser-Doppler Technique* (New York: Wiley)

[84] Tropea C 1995 Laser Doppler anemometry: recent developments and future challenges *Meas. Sci. Technol.* **6** 605–19

[85] Benard N and Moreau E 2010 Capabilities of the dielectric barrier discharge plasma actuator for multi-frequency excitations *J. Phys. D: Appl. Phys.* **43** 145201

[86] Benard N and Moreau E 2012 Role of the electric waveform supplying a dielectric barrier discharge plasma actuator *Appl. Phys. Lett.* **100** 193503

[87] Neumann M, Friedrich C, Czarske J, Kriegseis J and Grundmann S 2013 Determination of the phase-resolved body force produced by a dielectric barrier discharge plasma actuator *J. Phys. D: Appl. Phys.* **46** 042001

[88] Kriegseis J, Schwarz C, Tropea C and Grundmann S 2013 Velocity-information-based force-term estimation of dielectric-barrier discharge plasma actuators *J. Phys. D: Appl. Phys.* **46** 055202

[89] Willert C E and Gharib M 1991 Digital particle image velocimetry *Exp. Fluids* **10** 181–93

[90] Post M L 2004 Plasma actuators for separation control on stationary and unstationary airfoil *PhD Thesis* University of Notre Dame

[91] Santhanakrishnan A and Jacob J D 2007 Flow control with plasma synthetic jet actuators *J. Phys. D: Appl. Phys.* **40** 637–51

[92] Kim W, Do H, Mungal M G and Cappelli M A 2007 On the role of oxygen in dielectric barrier discharge actuation of aerodynamic flows *Appl. Phys. Lett.* **91** 181501

[93] Balcon N, Benard N and Moreau E 2009 Formation process of the electric wind produced by a plasma actuator *IEEE Trans. Dielectr. Electr. Insul.* **16** 463–9

[94] Kriegseis J, Dehler T, Gnirss M and Tropea C 2010 Common-base proper orthogonal decomposition as a means of quantitative data comparison *Meas. Sci. Technol.* **21** 085403

[95] Dedrick J, Im S, Cappelli M A, Boswell R W and Charles C 2013 Surface discharge plasma actuator driven by a pulsed 13.56 MHz–5 kHz voltage waveform *J. Phys. D: Appl. Phys.* **46** 405201

[96] Santhanakrishnan A, Reasor D A and LeBeau R P Jr 2009 Characterization of linear plasma synthetic jet actuators in an initially quiescent medium *Phys. Fluids* **21** 043602

[97] Kotsonis M, Ghaemi S, Veldhuis L and Scarano F 2011 Measurement of the body force field of plasma actuators *J. Phys. D: Appl. Phys.* **44** 045204

[98] Adrian R J 2005 Twenty years of particle image velocimetry *Exp. Fluids* **39** 159–69

[99] Humble R A, Craig S A, Vadyak J, McClure P D, Hofferth J W and Saric W S 2013 Spatiotemporal structure of a millimetric annular dielectric barrier discharge plasma actuator *Phys. Fluids* **25** 017103

[100] Kotsonis M and Ghaemi S 2011 Forcing mechanisms of dielectric barrier discharge plasma actuators at carrier frequency of 625 Hz *J. Appl. Phys.* **110** 113301

[101] Kotsonis M and Ghaemi S 2012 Performance improvement of plasma actuators using asymmetric high voltage waveforms *J. Phys. D: Appl. Phys.* **45** 045204

[102] Boucinha V, Magnier P, Leroy-Chesneau A, Weber R, Joussot R, Dong B and Hong D 2008 Characterization of the ionic wind induced by a sine DBD actuator used for laminar-to-turbulent transition delay *4th AIAA Flow Control Conf.*

[103] Hamdi M, Havet M, Rouaud O and Tarlet D 2014 Comparison of different tracers for PIV measurements in EHD airflow *Exp. Fluids* **55** 1–2

[104] Debien A, Benard N, David L and Moreau E 2012 Unsteady aspect of the electrohydrodynamic force produced by surface dielectric barrier discharge actuators *Appl. Phys. Lett.* **100** 013901

[105] Debien A, Benard N and Moreau E 2012 Streamer inhibition for improving force and electric wind produced by DBD actuators *J. Phys. D: Appl. Phys.* **45** 215201

[106] Murphy J P, Kriegseis J and Lavoie P 2013 Scaling of maximum velocity, body force, and power consumption of dielectric barrier discharge plasma actuators via particle image velocimetry *J. Appl. Phys.* **113** 243301

[107] Melling A 1997 Tracer particles and seeding for particle image velocimetry *Meas. Sci. Technol.* **8** 1406–16

[108] Rivir R, White A, Carter C, Ganguly B, Jacob J, Forelines A and Crafton J 2004 AC and pulsed plasma flow control *AIAA Paper* pp 9494–502

[109] Stephen E, Campbell A, Nygard J, Selby M, Hennig C and McLaughlin T 2011 Assessment of a corner plasma actuator for flow control using periodic jets *29th AIAA Applied Aerodynamics Conf. 2011*

[110] Durscher R and Roy S 2012 Evaluation of thrust measurement techniques for dielectric barrier discharge actuators *Exp. Fluids* **53** 1165–76

[111] Masati A, Sydney A J and Sedwick R J 2014 Parametric study of particle size for plasma actuator PIV measurements *52nd AIAA Aerospace Sciences Meeting: AIAA Science and Technology Forum and Exposition, SciTech 2014*

[112] Moreau E, Sosa R and Artana G 2008 Electric wind produced by surface plasma actuators: a new dielectric barrier discharge based on a three-electrode geometry *J. Phys. D: Appl. Phys.* **41** 115204–12

[113] Cristofolini A, Neretti G, Roveda F and Borghi C A 2012 Schlieren imaging in a dielectric barrier discharge actuator for airflow control *J. Appl. Phys.* **111** 033302

[114] Sosa R, Arnaud E, Memin E and Artana G 2009 Study of the flow induced by a sliding discharge *IEEE Trans. Dielectr. Electr. Insul.* **16** 305–11

[115] Opaits D F, Zaidi S S, Shneider M N, Miles R B, Likhanskii A V and Macheret S O 2009 Suppression of dielectric barrier discharge charge buildup using a partially conducting thin film *39th AIAA Fluid Dynamics Conf.*

[116] Dickerson R R and Stedman D H 1979 Qualitative and quantitative flow visualization technique using ozone *Rev. Sci. Instrum.* **50** 705–7

[117] Durscher R, Stanfield S and Roy S 2012 Characterization and manipulation of the saturation effect by changing the surface temperature of a dielectric barrier discharge actuator *Appl. Phys. Lett.* **101** 252902

[118] Enloe C L, McLaughlin T E, VanDyken R D, Kachner K D, Jumper E J and Corke T C 2004 Mechanisms and responses of a single dielectric barrier plasma actuator: plasma morphology *AIAA J.* **42** 589–94

[119] Van Dyken R, McLaughlin T E and Enloe C L 2004 Parametric investigations of a single dielectric barrier

plasma actuator *42nd AIAA Aerospace Sciences Meeting and Exhibit* pp 9503–14

[120] Hoskinson A R, Hershkowitz N and Ashpis D E 2008 Force measurements of single and double barrier DBD plasma actuators in quiescent air *J. Phys. D: Appl. Phys.* **41** 245209

[121] Cheong M, Greig A, Gibson B and Arjomandi M 2011 An investigation into the effect of electric field on the performance of dielectric barrier discharge plasma actuators *Exp. Therm. Fluid Sci.* **35** 1600–7

[122] Kriegseis J, Grundmann S and Tropea C 2011 Power consumption, discharge capacitance and light emission as measures for thrust production of dielectric barrier discharge plasma actuators *J. Appl. Phys.* **110** 013305

[123] Pereira R, Ragni D and Kotsonis M 2014 Effect of external flow velocity on momentum transfer of dielectric barrier discharge plasma actuators *J. Appl. Phys.* **116** 103301

[124] Ashpis D E and Laun M C 2014 Dielectric barrier discharge (DBD) plasma actuators thrust: measurement methodology incorporating new anti-thrust hypothesis *52nd AIAA Aerospace Sciences Meeting: AIAA Science and Technology Forum and Exposition, SciTech 2014*

[125] Versailles P, Gingras-Gosselin V and Vo H D 2010 Impact of pressure and temperature on the performance of plasma actuators *AIAA J.* **48** 859–63

[126] Abe T, Takizawa Y, Sato S and Kimura N 2008 Experimental study for momentum transfer in a dielectric barrier discharge plasma actuator *AIAA J.* **46** 2248–56

[127] Enloe C L, McHarg M G and McLaughlin T E 2008 Time-correlated force production measurements of the dielectric barrier discharge plasma aerodynamic actuator *J. Appl. Phys.* **103** 073302

[128] Font G I, Enloe C L, Newcomb J Y, Teague A L, Vasso A R and McLaughlin T E 2011 Effects of oxygen content on dielectric barrier discharge plasma actuator behavior *AIAA J.* **49** 1366–73

[129] Elias P Q and Castera P 2013 Measurement of the impulse produced by a pulsed surface discharge actuator in air *J. Phys. D: Appl. Phys.* **46** 365204

[130] Debien A, Benard N, David L and Moreau E 2012 Erratum: Unsteady aspect of the electrohydrodynamic force produced by surface dielectric barrier discharge actuators (2012 *Appl. Phys. Lett.* **100** 013901) *Appl. Phys. Lett.* **101** 229903

[131] Noca F, Shiels D and Jeon D 1997 Measuring instantaneous fluid dynamic forces on bodies, using only velocity fields and their derivatives *J. Fluids Struct.* **11** 345–50

[132] Wilke J B 2009 Aerodynamic flow-control with dielectric barrier discharge plasma actuators Number 19 in DLR Deutsches Zentrum fur Luft- und Raumfahrt e.V. - Forschungsberichte

[133] Van Oudheusden B W 2013 PIV: based pressure measurement *Meas. Sci. Technol.* **24** 032001

[134] Ragni D, Ashok A, Van B W and Scarano F 2009 Surface pressure and aerodynamic loads determination of a transonic airfoil based on particle image velocimetry *Meas. Sci. Technol.* **20** 074005

[135] Benard N, Debien A and Moreau E 2013 Time-dependent volume force produced by a non-thermal plasma actuator from experimental velocity field *J. Phys. D: Appl. Phys.* **46** 245201

[136] Albrecht T, Weier T, Gerbeth G, Metzkes H and Stiller J 2011 A method to estimate the planar, instantaneous body force distribution from velocity field measurements *Phys. Fluids* **23** 021702

[137] Patankar S V and Spalding D B 1972 A calculation procedure for heat, mass and momentum transfer in three-dimensional parabolic flows *Int. J. Heat Mass Transfer* **15** 1787–806

[138] Enloe C L, McLaughlin T E, Font G I and Baughn J W 2006 Parameterization of temporal structure in the single-dielectric-barrier aerodynamic plasma actuator *AIAA J.* **44** 1127–36

[139] Tirumala R, Benard N, Moreau E, Fenot M, Lalizel G and Dorignac E 2014 Temperature characterization of dielectric barrier discharge actuators: influence of electrical and geometric parameters *J. Phys. D: Appl. Phys.* **47** 255203

[140] Meola C and Carlomagno G M 2004 Recent advances in the use of infrared thermography *Meas. Sci. Technol.* **15** R27–R58

[141] Joussot R, Hong D, Rabat H, Boucinha V, Weber-Rozenbaum R and Leroy-Chesneau A 2010 Thermal characterization of a DBD plasma actuator: dielectric temperature measurements using infrared thermography *40th AIAA Fluid Dynamics Conf.*

[142] Neretti G, Cristofolini A, Borghi C A, Gurioli A and Pertile R 2012 Experimental results in DBD plasma actuators for air flow control *IEEE Trans. Plasma Sci.* **40** 1678–87

[143] Kriz G S and Lampman G M 2009 *Introduction to Spectroscopy* (Belmont, CA: Brooks/Cole)

[144] Dedrick J, WBoswell R and Charles C 2010 Asymmetric surface barrier discharge plasma driven by pulsed 13.56 MHz power in atmospheric pressure air *J. Phys. D: Appl. Phys.* **43** 342001

[145] Gulec A, Oksuz L and Hershkowitz N 2011 Optical studies of dielectric barrier plasma aerodynamic actuators *Plasma Sources Sci. Technol.* **20** 045019

[146] Biganzoli I, Barni R, Riccardi C, Gurioli A and Pertile R 2013 Optical and electrical characterization of a surface dielectric barrier discharge plasma actuator *Plasma Sources Sci. Technol.* **22** 025009

[147] Stanfield S A and Menart J 2013 Optical emission spectroscopy measurements within a single microdischarge of a dielectric barrier discharge actuator *Appl. Phys. Lett.* **103** 054106

[148] www.specair-radiation.net/

[149] Opaits D F, Likhanskii A V, Neretti G, Zaidi S, Shneider M N, Miles R B and MacHeret S O 2008 Experimental investigation of dielectric barrier discharge plasma actuators driven by repetitive high-voltage nanosecond pulses with dc or low frequency sinusoidal bias *J. Appl. Phys.* **104** 043304

[150] Benard N, Zouzou N, Claverie A, Sotton J and Moreau E 2012 Optical visualization and electrical characterization of fast-rising pulsed dielectric barrier discharge for airflow control applications *J. Appl. Phys.* **111** 033303

[151] Dawson R and Little J 2013 Characterization of nanosecond pulse driven dielectric barrier discharge plasma actuators for aerodynamic flow control *J. Appl. Phys.* **113** 103302

[152] Correale G, Michelis T, Ragni D, Kotsonis M and Scarano F 2014 Nanosecond-pulsed plasma actuation in quiescent air and laminar boundary layer *J. Phys. D: Appl. Phys.* **47** 105201

[153] Takashima K, Zuzeek Y, Lempert W R and Adamovich I V 2011 Characterization of a surface dielectric barrier discharge plasma sustained by repetitive nanosecond pulses *Plasma Sources Sci. Technol.* **20** 055009

[154] Pons J, Rabat H, Leroy A and Hong D 2014 Experimental study of a surface dbd actuator supplied by an atypical nanosecond rising high-voltage pulse *IEEE Trans. Plasma Sci.* **42** 1661–8

[155] Kogelschatz U 2003 Filamentary, patterned, and diffuse barrier discharges *IEEE Trans. Plasma Sci.* **30** 1400–8

[156] Enloe C L, McLaughlin T E, VanDyken R D, Kachner K D, Jumper E J, Corke T C, Post M and Haddad O 2004 Mechanisms and responses of a single dielectric barrier plasma actuator: geometric effects *AIAA J.* **42** 595–604

[157] Sasoh A, Kikuchi K and Sakai T 2007 Spatio-temporal filament behaviour in a dielectric barrier discharge plasma actuator *J. Phys. D: Appl. Phys.* **40** 4181–4

[158] Opaits D F, Shneider M N, Miles R B, Likhanskii A V and MacHeret S O 2008 Surface charge in dielectric barrier discharge plasma actuators *Phys. Plasmas* **15** 073505

[159] Giepman R H M and Kotsonis M 2011 On the mechanical efficiency of dielectric barrier discharge plasma actuators *Appl. Phys. Lett.* **98** 221504

[160] Joussot R, Boucinha V, Weber R and Hong D 2011 Negative spark leaders on a surface DBD plasma actuator *IEEE Trans. Plasma Sci.* **39** 2194–5

[161] Kriegseis J, Müller B, Grundmann S and Tropea C 2011 Capacitance and power consumption quantification of dielectric barrier discharge (DBD) plasma actuators *J. Electrost.* **69** 302–12

[162] Ashpis D E, Laun M C and Griebeler E L 2012 Progress toward accurate measurements of power consumptions of DBD plasma actuators *50th AIAA Aerospace Sciences Meeting Including the New Horizons Forum and Aerospace Exposition*

[163] Ndong A C A, Zouzou N, Benard N and Moreau E 2013 Geometrical optimization of a surface DBD powered by a nanosecond pulsed high voltage *J. Electrost.* **71** 246–53

[164] Cristofolini A, Neretti G and Borghi C A 2013 Effect of the charge surface distribution on the flow field induced by a dielectric barrier discharge actuator *J. Appl. Phys.* **114** 073303

[165] Cristofolini A, Borghi C A and Neretti G 2013 Charge distribution on the surface of a dielectric barrier discharge actuator for the fluid-dynamic control *J. Appl. Phys.* **113** 143307

[166] Jiang H, Shao T, Zhang C, Li W, Yan P, Che X and Schamiloglu E 2013 Experimental study of Q-V lissajous figures in nanosecond-pulse surface discharges *IEEE Trans. Dielectr. Electr. Insul.* **20** 1101–11

[167] Nichols T G and Rovey J L 2013 Surface potential and electric field measurements in plasma actuators at low pressure *AIAA J.* **51** 1054–65

[168] Pang L, He K, Di D, Zhang Q and Liu C 2014 Capacitances and energy deposition curve of nanosecond pulse surface dielectric barrier discharge plasma actuator *Rev. Sci. Instrum.* **85** 053501

[169] Tumanski S 2007 Induction coil sensors: a review *Meas. Sci. Technol.* **18** R31–R46

[170] Manley T C 1943 The electric characteristics of the ozonator discharge *Trans. Electrochem. Soc.* **84** 83–96

[171] Lawrence N Dworsky 1980 *Modern Transmission Line Theory and Applications* (Malabar, FL: Krieger)

[172] Zhang Q, Zhu J, Jia J, Tao F and Yang L 2006 Design of a current transducer with a magnetic core for use in measurements of nanosecond current pulses *Meas. Sci. Technol.* **17** 895–900

[173] Hershkowitz N, Lutfi O and Hoskinson A 2009 Optical comparison of single and double dielectric barrier plasma actuators *51st Annual Meeting of the APS Division of Plasma Physics* vol 54

[174] Ashpis D E and Thurman D R 2011 Test conditions for performance characterization of dielectric barrier discharge (DBD) plasma actuators for active flow control in jet engines *Proc. ASME Turbo Expo* **1** 389–415

[175] Labergue A, Leger L, Moreau E, Touchard G and Bonnet J 2004 Experimental study of the detachment and the reattachment of an airflow along an inclined wall controlled by a surface corona discharge-application to a plane turbulent mixing layer *IEEE Trans. Ind. Appl.* **40** 1205–14

[176] Pavon S, Dorier J, Hollenstein Ch, Ott P and Leyland P 2007 Effects of high-speed airflows on a surface dielectric barrier discharge *J. Phys. D: Appl. Phys.* **40** 1733–41

[177] Benard N, Balcon N and Moreau E 2008 Electric wind produced by a surface dielectric barrier discharge operating in air at different pressures: aeronautical control insights *J. Phys. D: Appl. Phys.* **41** 042002

[178] Benard N, Balcon N and Moreau E 2009 Electric wind produced by a surface dielectric barrier discharge operating over a wide range of relative humidity *47th AIAA Aerospace Sciences Meeting including the New Horizons Forum and Aerospace Exposition*

[179] Hollick M M, Arjomandi M and Cazzolato B S 2011 An investigation into the sensory application of DBD plasma actuators for pressure measurement *Sensors Actuators* **171** 102–8

[180] Erfani R, Zare-Behtash H and Kontis K 2012 Plasma actuator: influence of dielectric surface temperature *Exp. Therm. Fluid Sci.* **42** 258–64

[181] Erfani R, Zare-Behtash H and Kontis K 2012 Influence of shock wave propagation on dielectric barrier discharge plasma actuator performance *J. Phys. D: Appl. Phys.* **45** 225201

[182] Khramtsov P P, Penyazkov O G, Grishchenko V M, Chernik M Y, Shatan I N and Shikh I A 2012 Characteristic features of a barrier discharge occurring on the Zhukovskii aerofoil on variation of the surrounding air pressure *J. Eng. Phys. Thermophys.* **85** 382–7

[183] Kriegseis J, Grundmann S and Tropea C 2012 Airflow influence on the discharge performance of dielectric barrier discharge plasma actuators *Phys. Plasmas* **19** 073509

[184] Valerioti J A and Corke T C 2012 Pressure dependence of dielectric barrier discharge plasma flow actuators *AIAA J.* **50** 1490–502

[185] Aba'A Ndong A C, Zouzou N, Benard N and Moreau E 2013 Effect of dielectric aging on the behavior of a surface nanosecond pulsed dielectric barrier discharge *IEEE Trans. Dielectr. Electr. Insul.* **20** 1554–60

[186] Pereira R, Ragni D and Kotsonis M 2013 The effect of external flow velocity on the momentum transfer of DBD plasma actuators *44th AIAA Plasmadynamics and Lasers Conf.*

[187] Kriegseis J, Grundmann S and Tropea C 2013 Performance reduction of dielectric barrier discharge plasma actuators at higher mach numbers *Notes Numer. Fluid Mech. Multidiscip. Des.* **121** 209–17

[188] Wu Y, Li Y, Jia M, Song H and Liang H 2013 Effect of pressure on the emission characteristics of surface dielectric barrier discharge plasma *Sensors Actuators* **203** 1–5

[189] Kriegseis J, Barckmann K, Frey J, Tropea C and Grundmann S 2014 Competition between pressure effects and airflow influence for the performance of plasma actuators *Phys. Plasmas* **21** 053511

[190] Wilkinson S P, Siochi E, Sauti G, Xu T, Meador A and Guo H 2014 Evaluation of dielectric-barrier-discharge actuator substrate materials *45th AIAA Plasmadynamics and Lasers Conf.* pp 2014–810

[191] Adrian R J and Westerweel J 2011 *Particle Image Velocimetry* (Cambridge: Cambridge University Press)

[192] Ragni D, Schrijer F, Van Oudheusden B W and Scarano F 2011 Particle tracer response across shocks measured by PIV *Exp. Fluids* **50** 53–64

[193] Miles R B 2015 Optical diagnostics for high-speed flows *Prog. Aerosp. Sci.* **72** 30–6

[194] Font G I, Enloe C L and McLaughlin T E 2010 Plasma volumetric effects on the force production of a plasma actuator *AIAA J.* **48** 1869–74